BRANCHED CAUCHY-RIEMANN STRUCTURES ON ONCE-PUNCTURED TORUS BUNDLES[*]

ALEX CASELLA[†]

Abstract. Unlike in hyperbolic geometry, the monodromy ideal triangulation of a hyperbolic once-punctured torus bundle M_f has no natural geometric realization in Cauchy-Riemann (CR) space. By introducing a new type of 3–cell, we construct a different cell decomposition $\mathcal{D}_f$ of M_f that is always realisable in CR space. As a consequence, we show that every hyperbolic once-punctured torus bundle admits a branched CR structure, whose branch locus is contained in the union of all edges of $\mathcal{D}_f$. Furthermore, we explicitly compute the ramification order around each component of the branch locus and analyse the corresponding holonomy representations.

Key words. Geometric Structures, Cauchy, Riemann, Torus Bundles, Ideal Triangulations, Branching.

Mathematics Subject Classification. 57M50, 32V05.

1. Introduction. A *geometry* or *geometric structure* (G, X) is a homogeneous space X together with a transitive action on X by a Lie group G, which acts as the symmetry group of the geometry. This concept was originally introduced by Klein in his celebrated Erlangen program [18], and rapidly developed by Ehresmann [7] and many others afterwards. When X and G are chosen appropriately, one recovers many classical geometries like hyperbolic $(\mathrm{SO}(1, n), \mathbb{H}^n)$, Euclidean $(\mathbb{R}^n \rtimes \mathrm{O}(n), \mathbb{E}^n)$ or spherical $(\mathrm{O}(n+1), \mathbb{S}^n)$ geometry. A (G, X)–manifold M is a manifold endowed with a (G, X)–structure, namely an atlas of charts in the model space X, whose transition functions are restrictions of elements of G.

As more and more connections between topology and geometry were discovered, (G, X)–structures have become a central topic in the study of manifolds. Among many contributors, William Thurston is one of the most celebrated pioneers. In [27], he develops a way to construct hyperbolic structures on cusped 3–manifolds using *ideal triangulations*, namely decompositions into tetrahedra whose vertices are removed. The strategy consists in realising these simple pieces as hyperbolic objects, that glue up coherently in the manifold M. Consistency of the gluings can be encoded in a system of complex valued equations, whose solutions correspond to hyperbolic structures on M. Since Thurston, many authors have studied and further developed his technique ([5], [6], [12], [22], [26], [30], et al.).

In two recent papers ([8], [9]), a similar strategy was employed to construct branched Cauchy-Riemann structures (CR in short) on the complement of the figure eight knot. CR geometry is modelled on the three-sphere $\mathbb{S}^3 \subset \mathbb{C}^2$, with the contact structure obtained by the intersection $Y = T\mathbb{S}^3 \cap JT\mathbb{S}^3$, where J is the multiplication by i in $\mathbb{C}^2$ (see for example [2]). The operator J restricted to Y defines the standard CR structure on $\mathbb{S}^3$. Its group of CR automorphisms is $\mathrm{PU}(2, 1)$, thus a manifold M has a (spherical) CR structure when it is endowed with a geometric $(\mathrm{PU}(2, 1), \mathbb{S}^3)$–structure. The fact that every 3–manifold admits a contact structure [21] suggests that CR geometry has the potential to play an important role in three dimensional topology. Nevertheless, only few examples of CR manifolds are known. Most of them are closed Seifert fibred manifolds [17] or obtained by Dehn surgery from the White-

---

head link [24, 25]. On the other hand, some examples of 3–manifolds which have no CR structures are known [13].

Every CR structure on a manifold M comes with a *developing map* $\widetilde{M} \to \mathbb{S}^3$ and a *holonomy representation* $\pi_1(M) \to \mathrm{PU}(2,1)$ (cf. §5). This leads to the following classical problem:

QUESTION 1. *Given a representation* $\rho : \pi_1(M) \to \mathrm{PU}(2,1)$, *is there a CR structure on* M *whose holonomy is* ρ?

In general, this can be a challenging task. Inspired by the work of Falbel in [8], one may tackle this problem with a more general notion of CR structures, by allowing branching. Charts are not diffeomorphisms anymore, but locally branched coverings. By relaxing this condition, one obtains a geometric structure whose developing map is locally injective everywhere except for a nowhere-dense set, the branch locus. Nevertheless the associated holonomy representation is into $\mathrm{PU}(2,1)$, thus one can ask a similar question:

QUESTION 2. *Given a representation* $\rho : \pi_1(M) \to \mathrm{PU}(2,1)$, *is there a* branched *CR structure on* M *whose holonomy is* ρ?

On the other hand, branched CR structures are yet to be explored. The goal of this paper is to provide an interesting technique to concretely construct branched CR structures for a large class of 3–manifolds.

The spaces we investigate here are *once-punctured torus bundles*, orientable manifolds which are the interior of compact 3–manifolds with boundary a torus. They are fiber bundles over the circle, with fiber space a once-punctured torus. The figure eight knot complement is one such example. Most of these manifolds are hyperbolic [23], and exhibit important combinatorial properties. In particular, Floyd and Hatcher showed that each hyperbolic once-punctured torus bundle admits a canonical realization as an ideal triangulation, called the *monodromy ideal triangulation* [11]. This type of triangulation is part of a larger class of fundamental triangulations called *veering triangulations*, developed by Agol in [1]. The importance of this decomposition relies on its rich combinatorial structure, but also on its geometric properties. For example, Lackenby showed it to be geometrically canonical in the sense of Epstein-Penner [19], while Guéritaud used it to recover Thurston's hyperbolicity of once-punctured torus bundles [15].

In this paper we modify the monodromy ideal triangulation of each once-punctured torus bundle to a new ideal cell decomposition, that is geometrically realisable in CR space, and whose set of edges contains the branch locus. This decomposition is made up of tetrahedra and 3–cells that we call *slabs*, CW complexes obtained by deformation retracting the base of a square pyramid onto one of its sides. In the case of the figure eight knot complement, Falbel [8] uses one of these slabs implicitly, as part of a *generalised tetrahedron*, but the CR structure thus constructed consists of charts that are not embeddings of the tetrahedra. In particular, there is a small neighbourhood of one edge in a tetrahedron that develops to a flat bigon. This is not an obstruction in Falbel's proof: he focuses on the union of the images of two specific charts and shows that its quotient by the face pairings is homeomorphic to the figure eight knot complement. This strategy is hard to generalise to other punctured torus bundles and it is somehow unnatural. For example, it is true only for the figure eight knot complement that the branch locus occurs precisely at the edges of the triangulation. This suggests the use of a more suitable cell decomposition, such that we can geometrically realise each ideal cell by embedding it in CR space. For this to

work, six geometrically different types of slabs will be defined. Each construction is very explicit and calculations are done directly in coordinates in the CR sphere. A collection of the main results is summarised in the following theorem.

THEOREM 1. *Let M_f be a hyperbolic once-punctured torus bundle. Then M_f admits an ideal cell decomposition $\mathcal{D}_f$ that is geometrically realisable in CR space. It corresponds to a branched CR structure, whose branch locus is contained in the union of all edges of $\mathcal{D}_f$.*

Moreover, the ramification order around each edge e only depends on the valence of e in $\mathcal{D}_f$, and it is explicitly computable.

The construction presented in this paper has the potential to further extend to more general punctured surface bundles, as they also admit layered triangulations. Although the realisability of the cell decomposition $\mathcal{D}_f$ seems to rely on the fact that the base surface is a once-punctured torus, we intend to address this problem in future work using the veering triangulations of Agol [1].

The content of this paper is organised as follows. In sections 2 and 3 we review background material on once-punctured torus bundles and monodromy ideal triangulations. They mostly serve to set notations and underline the most relevant properties. CR geometry is covered in §4. There we define CR tetrahedra and slabs, the two fundamental 3–cells which will be the building blocks of the CR structures in §5. Section 5 is the core of the paper, where we introduce the notion of branched CR structures and prove Theorem 1, first in the explicit case of the figure eight knot, then in the general case for all once-punctured torus bundles. We conclude by computing ramification orders of the branch locus and a brief analysis of the holonomy representations in §6. In particular, the very last section 6.2 is a summary of some facts about the holonomy representations and the connection to the work of Fock and Goncharov on positive representations [12], mostly for experts.

2. Once-punctured torus bundles. Let $\mathbb{T}_0 := \left(\mathbb{R}^2 \setminus \mathbb{Z}^2\right)/\mathbb{Z}^2$ be the once-punctured torus endowed with its standard differential structure and standard orientation. The *mapping class group* of $\mathbb{T}_0$ is the group $\mathrm{MCG} = \mathrm{MCG}(\mathbb{T}_0)$ of isotopy classes of orientation preserving diffeomorphisms $f : \mathbb{T}_0 \to \mathbb{T}_0$. For $[f] \in \mathrm{MCG}$, the *once-punctured torus bundle M_f* is the differentiable oriented 3–manifold

$$M_f := \mathbb{T}_0 \times [0,1]/ \sim,$$

where $(x, 0) \sim (f(x), 1)$ for $x \in \mathbb{T}_0$. The manifold M_f is a surface bundle over the circle, with fiber space $\mathbb{T}_0$, well-defined up to diffeomorphism.

The natural identification of $\mathbb{T}_0$ with the square spanned by the standard basis of $\mathbb{R}^2$ induces an isomorphism $\mathrm{MCG} \cong \mathrm{SL}(2, \mathbb{Z})$, hence each map $[f] \in \mathrm{MCG}$ has well-defined eigenvalues in $\mathbb{C}$ (cf. [10]). The following characterization is fundamental to study the geometry of M_f, as for example it helps discerning hyperbolic bundles.

THEOREM 2 (Thurston, 1996 [23]). *M_f admits a finite volume, complete hyperbolic metric if and only if $[f]$ has two distinct real eigenvalues.*

The element $[f]$ has distinct real eigenvalues if and only if $(\mathrm{tr}[f])^2 > 4$. If the trace is in $\{-1, 0, 1\}$, then $[f]$ has finite order and M_f is Seifert fibred. While if $\mathrm{tr}[f] = \pm 2$, then f preserves a non-trivial simple closed curve in the punctured torus, which defines an incompressible torus or Klein bottle in M_f. In both cases we get an obstruction to the existence of the hyperbolic metric. An elementary and constructive proof of the other cases can be found in [15].

3. The monodromy ideal triangulation. In this section we recall the canonical realization of a hyperbolic once-punctured torus bundle M_f as an ideal triangulation, as described by Floyd and Hatcher in [11], called the *monodromy ideal triangulation* of M_f. For M_f hyperbolic, Theorem 2 implies that the eigenvalues of $[f]$ are distinct with the same sign. To simplify the construction, we are going to make the further assumption that the eigenvalues are positive. This will not cause any loss of generality: if $[f]$ has two negative eigenvalues, then $[-f]$ has positive eigenvalues, and the monodromy triangulation of M_f can be easily deduced from the monodromy triangulation of M_{-f}. See Remark 4 for more details.

3.1. Flip sequence. An *ideal triangulation* $\mathcal{T}$ of $\mathbb{T}_0$ is a maximal collection of pairwise disjoint and non-homotopic (relative the puncture) essential arcs. Every ideal triangulation of $\mathbb{T}_0$ comprises three essential arcs, called *ideal edges*, and divides the surface into two *ideal triangles*. All of these ideal triangulations are combinatorially equivalent, but they can be distinguished by the fact that they are not isotopic via an isotopy fixing the puncture.

Without loss of generality, one can assume that ideal triangulations of $\mathbb{T}_0$ are *straight*, in the sense that each ideal edge is the intersection with $\mathbb{T}_0$ of the quotient of a straight line through the origin in $\mathbb{R}^2$. In a straight triangulation $\mathcal{T}$, the *slope* of an edge is the slope of the corresponding straight line. Since edges start and terminate at the puncture, their slopes must be rational, hence there is a bijection between ideal edges and $\mathbb{Q} \cup \{\infty\}$, by associating each edge to its slope.

The set of isotopy classes of ideal triangulations can be encoded as the vertices of the *Farey tree* F^*. This tree is dual to the *Farey tessellation* F (cf. Figure 1), a tessellation of the hyperbolic plane by ideal triangles. The ideal vertices of this tessellation are the set of slopes of ideal edges $\mathbb{Q} \cup \{\infty\}$ in the circle at infinity. In particular, the ideal vertices of a triangle in F correspond to the slopes of three disjoint non-homotopic properly embedded arcs in $\mathbb{T}_0$, and hence to an ideal triangulation. Thus, there is one vertex of the dual tree F^* for each isotopy class of ideal triangulation of the once-punctured torus, and every such ideal triangulation is uniquely determined by a triplet of slopes satisfying the Farey sum. A beautiful treatment of this topic can be found in [3].

By adopting the convention that 0 and ∞ are neither negative nor positive, we say that an ideal triangulation is *positive* (resp. *negative*) if at least one if its slopes is positive (resp. negative). The *standard positive* (resp. *negative*) *ideal triangulation* of $\mathbb{T}_0$ is the triangulation $\mathcal{T}_+$ (resp. $\mathcal{T}_-$) with slopes $\{0, 1, \infty\}$ (resp. $\{0, -1, \infty\}$).

Two vertices of the dual tree F^* are joined by an edge if and only if the corresponding ideal triangulations differ by a single slope. Passing from one triangulation to the other is usually called *edge flipping*, as it involves removing one edge, resulting in a square with side identifications, and then inserting the other diagonal of the square. As F^* is a tree, every two ideal triangulations of $\mathbb{T}_0$ differ by a unique minimal sequence of edge flips.

Edge flips are of three types, depending on the slope we are flipping over. A *right flip* $\mathcal{R}$ (resp. *left flip* $\mathcal{L}$) is an edge flip of the largest (resp. smallest) slope. The remaining flip will be referred to as a *middle flip* $\mathcal{M}$. For example, starting from the standard positive triangulation $\{0, 1, \infty\}$ of $\mathbb{T}_0$, a right flip produces the triangulation $\{0, \frac{1}{2}, 1\}$, a left flip gives $\{1, 2, \infty\}$, and a middle flip gives $\{0, -1, \infty\}$.

One can visualise the dynamics of edge flips on the dual tree F^* as follows. Let $\mathcal{T}_m$ be a positive ideal triangulation (different from the standard one) and let $\mathcal{T}_+, \mathcal{T}_1, \ldots, \mathcal{T}_{m-1}$ be the sequence of triangulations along the unique shortest path be-

tween the standard positive triangulation and $\mathcal{T}_m$. By definition, a middle flip kills the middle slope, hence it corresponds to a back-track towards $\mathcal{T}_+$ and transforms $\mathcal{T}_m$ into $\mathcal{T}_{m-1}$, contradicting the minimality of the path. If you exclude back-tracking, one can move along F^* in only two other ways, corresponding to a right or left flip. By orienting the hyperbolic plane with its standard positive orientation, a right (resp. left) flip corresponds exactly to turning right (resp. left) at $\mathcal{T}_m$ (cf. Figure 1). A perfectly analogous arguments works if we replace $\mathcal{T}_m$ with a negative ideal triangulation.
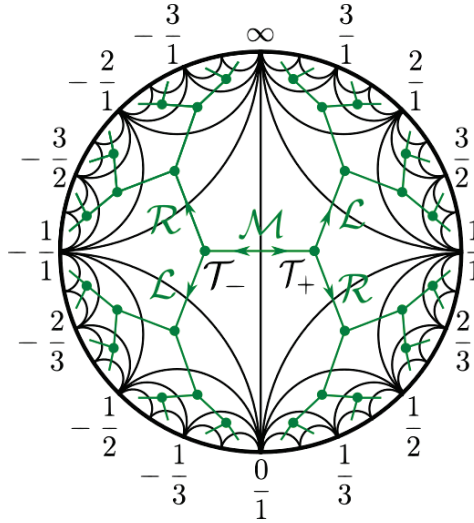

FIGURE 1. *The Farey tree is dual to the Farey tessellation of the hyperbolic plane. Every vertex corresponds to an ideal triangulation of the once-punctured torus, and every edge corresponds to an edge flip.*

The following lemma is a direct consequence of the above discussion.

LEMMA 3. *Let $\mathcal{T}$ be a positive (resp. negative) ideal triangulation different from the positive (resp. negative) standard one $\mathcal{T}_0$. The unique sequence of edge flips from $\mathcal{T}_0$ to $\mathcal{T}_m$ does not contain any middle flips. Conversely, the sequence of flips from $\mathcal{T}_m$ to $\mathcal{T}_0$ only contains middle flips.*

Let $f : \mathbb{T}_0 \to \mathbb{T}_0$ be a diffeomorphism of the once-punctured torus. The map f acts transitively on the set of ideal triangulations of $\mathbb{T}_0$, inducing an isomorphism of the Farey tree F^*. Every isomorphism of a simplicial tree has either a fixed point, or leaves invariant a unique copy of $\mathbb{R}$, called *axis*. The former case happens when $\text{tr}([f]) \in \{-1, 0, 1\}$ and the action is periodic. In the latter case, let V_0 be a vertex on the axis. The unique shortest path in F^* from V_0 to $f(V_0)$ runs along the axis, and naturally corresponds to a sequence of edge flips. When $\text{tr}([f])^2 = 4$, the axis has a unique endpoint on the boundary of the hyperbolic plane, and the action is parabolic. Finally we observe that $-f$ acts on F^* the same way as f, hence we will only consider automorphisms with distinct positive real eigenvalues.

After conjugating f, one can assume that V_0 corresponds to the standard positive ideal triangulation $\mathcal{T}_0$ and the axis does not run through any negative triangulation. It follows from Lemma 3 that $f(\mathcal{T}_0)$ differs from $\mathcal{T}_0$ by a unique sequence $\mathbf{w}_f$ of $\mathcal{R}$ (right) and $\mathcal{L}$ (left) flips. Furthermore, when the eigenvalues of f are distinct, $\mathbf{w}_f$

always contains at least one right flip and one left flip. In other words, there exist $a_j, b_j, k \in \mathbb{N}$ and $c \in \mathbb{N} \cup \{0\}$ such that

$$\mathbf{w}_f = \mathcal{R}^{a_0} \mathcal{L}^{b_0} \dots \mathcal{R}^{a_k} \mathcal{L}^{b_k} \mathcal{R}^c \qquad \text{or} \qquad \mathbf{w}_f = \mathcal{L}^{a_0} \mathcal{R}^{b_0} \dots \mathcal{L}^{a_k} \mathcal{R}^{b_k} \mathcal{L}^c.$$

We say that $\mathbf{w}_f$ is the *flip sequence* of f or of M_f. Its *length* is the total number of edge flips, namely its word length $c + \sum_{j=0}^{k}(a_j + b_j)$. Under the canonical isomorphism $\mathrm{MCG}(\mathbb{T}_0) \cong \mathrm{SL}_2(\mathbb{Z})$, a right flip and a left flip correspond to the matrices

$$[f_\mathcal{R}] = \begin{pmatrix} 1 & 1 \\ 0 & 1 \end{pmatrix} \qquad \text{and} \qquad [f_\mathcal{L}] = \begin{pmatrix} 1 & 0 \\ 1 & 1 \end{pmatrix}.$$

3.2. The triangulation. The following description of the monodromy ideal triangulation is adapted from [15].

The *standard ideal tetrahedron* σ is, topologically, a compact tetrahedron with its vertices removed. One can picture σ as a square with its two diagonals, as in Figure 2. Oriented simplices of σ are determined by an ordering of the vertices, hence we refer to them by the notation $\sigma(i), \sigma(ij), \sigma(ijk), \sigma(ijkl)$. Sometimes we use the same notation for the unoriented counterparts, but only when it is clear from the context that we ignore the orientation. By identifying the pair of opposite edges $\sigma(13), \sigma(24)$ and $\sigma(12), \sigma(34)$, the exterior of σ becomes the union of two *pleated surfaces*, homeomorphic to the once-punctured torus $\mathbb{T}_0$. The *top* pleated surface $\sigma(\mathbb{T}_0)_+$ is made up of the two ideal triangles $\sigma(143), \sigma(124)$, while the *bottom* pleated surface $\sigma(\mathbb{T}_0)_-$ is made up of the two ideal triangles $\sigma(123), \sigma(324)$. Thus the ideal triangulation of $\sigma(\mathbb{T}_0)_+$ is obtained from $\sigma(\mathbb{T}_0)_-$ by an edge flip along $\sigma(23)$.

Suppose $\mathbb{T}_0$ is endowed with some ideal triangulation $\mathcal{T}$. We say that the tetrahedron σ *layers* on $\mathbb{T}_0$ if the bottom pleated surface of σ is glued to $\mathbb{T}_0$ via an orientation-preserving combinatorial isomorphism, called the *layering*. Let e be an oriented edge of $\mathcal{T}$. We say that σ layers on $\mathbb{T}_0$ *along* e if the chosen layering identifies e with the edge $\sigma(23)$. In general, there are six possible ways to layer σ on $\mathbb{T}_0$, one for each oriented edge of $\mathcal{T}$. To simplify the notation we make a further distinction. We recall that we are identifying $\mathbb{T}_0$ with the square spanned by the standard basis of $\mathbb{R}^2$. We say that a layering of σ is a (*right*) $\mathcal{R}$ *layering* (resp. (*left*) $\mathcal{L}$ *layering*) if σ layers along the edge with largest (resp. smallest) slope, oriented towards (resp. away from) the origin in $\mathbb{T}_0$. The motivation behind this notation is clear: if σ right layers (resp. left layers) on $\mathbb{T}_0$, the ideal triangulations of $\sigma(\mathbb{T}_0)_+$ is obtained from $\sigma(\mathbb{T}_0)_-$ by a right flip (resp. left flip).
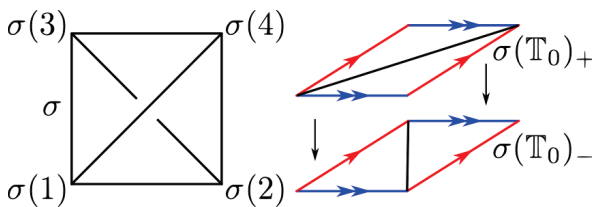

FIGURE 2. *The standard ideal tetrahedron σ and the two pleated surfaces $\sigma(\mathbb{T}_0)_+$ and $\sigma(\mathbb{T}_0)_-$.*
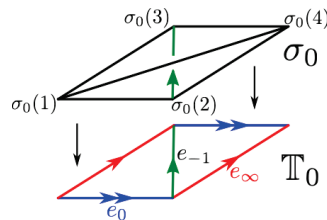
FIGURE 3. *A layering of the standard ideal tetrahedron along the edge e_{-1}.*

Let f be an element of $\mathrm{SL}_2(\mathbb{Z})$ with two distinct positive real eigenvalues and let $\mathbf{w}_f$ be the flip sequence of f. Suppose $\mathbf{w}_f$ has length m. Now we describe how

to construct the monodromy triangulation of the hyperbolic once-punctured torus bundle M_f. Suppose $\mathbb{T}_0$ is endowed with its negative standard ideal triangulation $\{0, -1, \infty\}$. Let σ_0 be a copy of the standard ideal tetrahedron layered on $\mathbb{T}_0$ along the edge of slope -1, oriented as in Figure 3. Then the top pleated surface $\sigma_0(\mathbb{T}_0)_+$ is triangulated as the positive standard ideal triangulation $\mathcal{T}_0$. For each letter $\mathcal{X}_j$ in $\mathbf{w}_f$, $j = 1, \ldots, m$, reading from left to right, we perform an $\mathcal{X}_j$ layering of a copy of the standard ideal tetrahedron σ_j on $\sigma_{j-1}(\mathbb{T}_0)_+$. The space obtained by stacking these tetrahedra is naturally homeomorphic to $\mathbb{T}_0 \times I$ [15, Section 3.2]. The last top pleated surface is $\sigma_m(\mathbb{T}_0)_+$. Its triangulation $\mathcal{T}_m$ is obtained from $\mathcal{T}_0$ by performing the sequence of edge flips $\mathbf{w}_f$. It follows that $\mathcal{T}_m = f(\mathcal{T}_0)$, and f induces an identification between σ_0 and σ_m which makes $\mathbb{T}_0 \times I$ into M_f. The *monodromy triangulation* of M_f is the ideal triangulation consisting of the tetrahedra $\sigma_0, \ldots, \sigma_{m-1}$ and the face pairings inherited from the layering construction. As an example, see the monodromy ideal triangulation of the figure eight knot complement in §5.2.

REMARK 4. *We remark that f and $-f$ act in the same way on the Farey tree, hence they share the same flip sequence. It follows that the monodromy triangulation of M_{-f} differs from the one of M_f only in the way σ_0 and σ_m are identified. More precisely, one can construct M_{-f} by composing the identification f between σ_0 and σ_m with the orientation preserving simplicial symmetry ι of σ_m swapping $\sigma_m(1)$ with $\sigma_m(4)$, and $\sigma_m(2), \sigma_m(3)$. Roughly speaking, the map ι is a rotation of σ_m by π preserving the two pleated surfaces.*

The layering construction induces a natural cyclic ordering of the tetrahedra, thus they will often be indexed modulo m. Similarly, one should think of the flip sequence $\mathbf{w}_f$ as a cyclic word, with a chosen starting point. For future reference, we introduce the following notation. A tetrahedron σ_j of the monodromy triangulation is said to be of *type* $\mathcal{R}$ (resp. *type* $\mathcal{L}$) if the *next* tetrahedron σ_{j+1} is layered on top of it by a right (resp. left) layering. We will sometimes record the type of σ_j by writing $\sigma_j^{\mathcal{R}}$ or $\sigma_j^{\mathcal{L}}$.

3.3. Combinatorics around the edges. Let $\mathcal{T}$ be the monodromy ideal triangulation of the once-punctured torus bundle M_f, and let m be the length of its flip sequence $\mathbf{w}_f$. Then $\mathcal{T}$ is made up of m tetrahedra $\sigma_0, \ldots, \sigma_{m-1}$, glued together by the layering construction. We denote by π the natural quotient map $\pi : \sqcup_j \sigma_j \to \mathcal{T} \cong M_f$, defined by the face pairings. The space M_f is the interior of a compact 3–manifold with torus boundary, so its Euler characteristic is zero. It follows that $\mathcal{T}$ has as many edges as tetrahedra, namely m. Nevertheless, each edge may be represented by multiple edges in each tetrahedron. The *valence* of an edge is the size of its inverse image under π. Roughly speaking, the valence of an edge e is the number of tetrahedra around e, counted with multiplicity.

We are now going to describe the local structure of the edges in $\mathcal{T}$. This will be useful in the analysis of the geometry around the edges in §5. We recall that each tetrahedron σ_j is a copy of the standard ideal tetrahedron σ via a canonical identification, hence it inherits labels at the vertices from σ.

Consider the edge $\sigma_0(14)$ of σ_0, and let $e_0 := \pi(\sigma_0(14))$ in $\mathcal{T}$. Suppose that $\sigma_0 = \sigma_0^{\mathcal{L}}$ is of type $\mathcal{L}$. Let $\sigma_1^{\mathcal{R}}, \ldots, \sigma_{n_0}^{\mathcal{R}}$, $n_0 \geq 0$, be the (possibly empty) sequence of tetrahedra of type $\mathcal{R}$ layered on top of $\sigma_0^{\mathcal{L}}$, such that $\sigma_{n_0+1}^{\mathcal{L}}$ is of type $\mathcal{L}$. This sequence corresponds to a subsequence $\mathcal{L}\mathcal{R}^{n_0}\mathcal{L}$ in the word $\mathbf{w}_f$ (thought of as a cyclic word). By definition, σ_1 left layers on σ_0, thus $\sigma_1(12), \sigma_1(34) \in \pi^{-1}(e_0)$. For every $2 \leq j \leq n_0 + 1$, the simplex σ_j right layers on σ_{j-1}, thus also $\sigma_j(12), \sigma_j(34) \in \pi^{-1}(e_0)$. Finally, σ_{n_0+2}

left layers on σ_{n_0+1}, closing up the sequence of tetrahedra around e_0 with the edge $\sigma_{n_0+2}(23)$. Locally around e_0, the tetrahedra $\sigma_0, \ldots, \sigma_{n_0+2}$ glue to form a *ribbon*, where σ_0 and σ_{n_0+2} appear once, while every other tetrahedron appears twice. See Figure 4 for a cross section of a neighbourhood of e_0. The simplex σ_0 (resp. σ_{n_0+2}) is the *bottom* (resp. *top*) of the ribbon, and every other simplex σ_j constitutes a *loop* on each side. We deduce that the valence of e_0 is $2n_0 + 4$.

An analogous picture arises when we assume that σ_0 is of type $\mathcal{R}$, with the difference that every tetrahedron of type $\mathcal{R}$ is now of type $\mathcal{L}$, and vice versa (cf. Figure 5). Furthermore, one may replace σ_0 with any other tetrahedron in $\mathcal{T}$ and make the same definitions. For future reference, we summarise all of the above in the following Lemma.

LEMMA 5. *Every edge e_j in $\mathcal{T}$ corresponds to a unique subsequence $\mathcal{L}\mathcal{R}^{n_j}\mathcal{L}$ or $\mathcal{R}\mathcal{L}^{n_j}\mathcal{R}$ in $\mathbf{w}_f$, $n_j \geq 0$, and a unique ribbon of tetrahedra $\sigma_j, \ldots, \sigma_{j+n_j+2}$. The simplex σ_j is the bottom of the ribbon, while σ_{j+n_j+2} is the top of the ribbon, and every other tetrahedron in between constitutes a loop on each side of the ribbon. Hence the valence of e_j is $2n_j + 4$.*

We remark that uniqueness of the ribbon follows from the fact that the bottom of the ribbon is the only tetrahedron in $\mathcal{T}$ whose edge (14) is a representative of e_j. Similarly, the top of the ribbon is the only tetrahedron whose edge (23) belongs to $\pi^{-1}(e_j)$. A simple counting argument shows that there is a bijection between the set of tetrahedra and the set of edges, thus associating every edge to its unique ribbon.
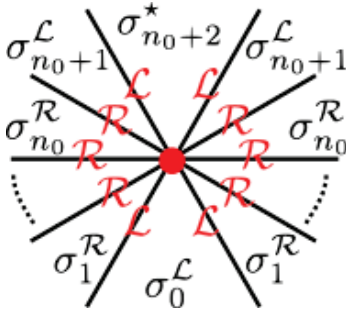

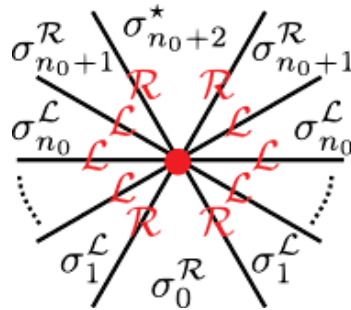FIGURE 4. *A cross section of the ribbon around e_0 for $\sigma_0 = \sigma_0^{\mathcal{L}}$.*

FIGURE 5. *A cross section of the ribbon around e_0 for $\sigma_0 = \sigma_0^{\mathcal{R}}$.*

4. CR Geometry. The *spherical Cauchy-Riemann geometry* is a (G,X)–geometry modelled on the *CR sphere*, namely the three-sphere $\mathbb{S}^3$ equipped with a natural $\mathrm{PU}(2,1)$ action. Unlike what we mentioned in the introduction, here we work with a definition of CR space that does not explicitly make use of contact geometry, but it underlines more clearly the action of $\mathrm{PU}(2,1)$. This point of view is going to be more suitable and relevant to our context. More details on the connection between CR geometry and contact geometry can be found in [2]. For more background material and proofs of the following Lemmas we refer the reader to [14, Section 4.3] or [16, Section 8].

The matrix group $\mathrm{U}(2,1)$ preserves the following Hermitian form of signature $(2,1)$ defined on the complex space $\mathbb{C}^3$:

$$\langle z, w \rangle := \overline{w}^t J z, \qquad \text{where} \qquad J := \begin{pmatrix} 0 & 0 & 1 \\ 0 & 1 & 0 \\ 1 & 0 & 0 \end{pmatrix}.$$

Let $\pi : \mathbb{C}^3 \setminus \{0\} \to \mathbb{CP}^2$ be the canonical projection, and consider the following sets in $\mathbb{C}^3$:

$$V_0 := \left\{ z \in \mathbb{C}^3 \setminus \{0\} \mid \langle z, z \rangle = 0 \right\}, \qquad V_- := \left\{ z \in \mathbb{C}^3 \mid \langle z, z \rangle < 0 \right\}.$$

Then $\mathbb{H}^2_{\mathbb{C}} := \pi(V_-)$ is the Siegel domain model of the *complex hyperbolic plane*. In the affine patch $\mathbb{C}^2 = \{[x, y, z] \in \mathbb{CP}^2 \mid z = 1\}$, the Siegel domain is the set defined by $2\Re(x) + |y|^2 < 0$. Its boundary is

$$\partial \mathbb{H}^2_{\mathbb{C}} := \pi(V_0) = \{[x, y, z] \in \mathbb{CP}^2 \mid x\bar{z} + |y|^2 + z\bar{x} = 0 \}.$$

As a topological space, $\partial \mathbb{H}^2_{\mathbb{C}}$ is homeomorphic to the three-sphere $\mathbb{S}^3$. The space $\mathbb{H}^2_{\mathbb{C}}$ has a natural complex structure and the projective group $\mathrm{PU}(2,1) := \mathrm{U}(2,1)/\lambda I$ is the group of its biholomorphic transformations. This is the *spherical model* of the CR sphere and the action of $\mathrm{PU}(2,1)$ on it is by *CR transformations*.

We are now going to describe a model for $\partial \mathbb{H}^2_{\mathbb{C}}$ which is particularly suitable for our framework. The *Heisenberg group* $\mathcal{H}$ is the space $\mathbb{C} \times \mathbb{R}$, equipped with the group law

$$(z_1, t_1) \cdot (z_2, t_2) := (z_1 + z_2, \ t_1 + t_2 + 2\Im(z_1 \overline{z_2})), \qquad z_1, z_2 \in \mathbb{C}, \quad t_1, t_2 \in \mathbb{R}.$$

In the formula above, $\Im(z)$ is the imaginary part of the complex number z. Using stereographic projection Λ, one can identify $\partial \mathbb{H}^2_{\mathbb{C}}$ with the one-point compactification $\overline{\mathcal{H}}$ of $\mathcal{H}$, thus obtaining the *Heisenberg model* of the CR sphere. In coordinates,

$$\Lambda : \begin{bmatrix} x \\ y \\ 1 \end{bmatrix} \mapsto \left(y, \frac{2x + |y|^2}{i} \right), \quad \Lambda^{-1} : (z, t) \mapsto \begin{bmatrix} \frac{it - |z|^2}{2} \\ z \\ 1 \end{bmatrix} \qquad \text{and} \qquad \Lambda : \begin{bmatrix} 1 \\ 0 \\ 0 \end{bmatrix} \mapsto \infty,$$

where $\Lambda : \partial \mathbb{H}^2_{\mathbb{C}} \to \overline{\mathcal{H}}$, $x, y, z \in \mathbb{C}$, and $t \in \mathbb{R}$. The action of $\mathrm{PU}(2,1)$ on $\overline{\mathcal{H}}$ is by defined by conjugating with Λ.

There are two kinds of totally geodesic submanifolds of real dimension two in $\mathbb{H}^2_{\mathbb{C}}$: complex geodesics and totally real geodesic planes. In this article we focus on complex geodesics. The boundary of a complex geodesic in $\partial \mathbb{H}^2_{\mathbb{C}}$ is a topological circle, called $\mathbb{C}$-*circle*. A $\mathbb{C}$-circle in $\overline{\mathcal{H}}$ is the image under Λ of a $\mathbb{C}$-circle in $\partial \mathbb{H}^2_{\mathbb{C}}$.

Lemma 6. *In the Heisenberg model $\overline{\mathcal{H}}$, a $\mathbb{C}$-circle is either a vertical line (vertical $\mathbb{C}$-circle) or an ellipse whose projection onto the z-plane is a circle (finite $\mathbb{C}$-circle).*

Vertical $\mathbb{C}$-circles always contain ∞, while finite $\mathbb{C}$-circles are fully contained in $\mathcal{H}$. We remark that a complex geodesic in $\mathbb{H}^2_{\mathbb{C}}$ is naturally endowed with a positive orientation given by its complex structure, hence every $\mathbb{C}$-circle also inherits an orientation.

Lemma 7. *CR transformations map $\mathbb{C}$-circles to $\mathbb{C}$-circles, preserving their orientations.*

Given two distinct points in Heisenberg space $\overline{\mathcal{H}}$, there is a unique $\mathbb{C}$-circle between them. We say that m points of $\overline{\mathcal{H}}$ are in *general position* if no three are contained in the same $\mathbb{C}$-circle. The group of CR transformations acts transitively on pairs of distinct points, while generic configurations of triples of points are parametrised by a real number. Given a cyclically ordered triple of points $(\!(P_1, P_2, P_3)\!)$ in $\overline{\mathcal{H}}$, its *Cartan angle* Å is

$$\text{Å}(P_1, P_2, P_3) := \arg(-\langle P'_1, P'_2 \rangle \langle P'_2, P'_3 \rangle \langle P'_3, P'_1 \rangle) \in \mathbb{R}, \qquad \text{where} \quad P'_j = \Lambda^{-1}(P_j).$$

LEMMA 8.   *Three points in $\overline{\mathcal{H}}$ are not in general position if and only if their Cartan angle is $\pm\frac{\pi}{2}$. Moreover, the group $\mathrm{PU}(2,1)$ acts simply transitively on ordered triples of points in general position with the same Cartan angle.*

4.1. CR Edges. Given two distinct points $P_1, P_2 \in \overline{\mathcal{H}}$, the *oriented edge* $[P_1, P_2]$ is the segment of the $\mathbb{C}$–circle between P_1 and P_2, oriented towards P_2. For example, the oriented edge $[(0,0), \infty]$ is the segment $\{(0,t) \in \overline{\mathcal{H}} \mid t > 0\}$, oriented towards ∞. Then $[P_1, P_2] \cup [P_2, P_1]$ is the whole $\mathbb{C}$–circle through P_1 and P_2. A topological disk in $\overline{\mathcal{H}}$ bounded by the loop $[P_1, P_2] \cup [P_2, P_1]$ will be referred to as a *bigon*.

4.2. CR Triangles. Suppose $P_1, P_2, P_3 \in \overline{\mathcal{H}}$ are three points in general position. For each pair, there are two possible oriented edges, for a total of eight choices of 1–skeletons defining a *triangle*. As $\overline{\mathcal{H}}$ is simply connected, we can always extend the 1–skeleton of a triangle to an embedded 2–cell, with boundary defined by that 1–skeleton. This can be done in many different ways, all equivalent up to isotopy. Inspired by the work of Falbel [8], we define the *marked triangles* $[P_1{}^+, P_2, P_3]$ and $[P_1{}^-, P_2, P_3]$ as foliations of oriented edges (cf. Figure 6):

$$[P_1{}^+, P_2, P_3] := \{P \in \overline{\mathcal{H}} \mid P \in [P_1, P_t] \ \text{ for } \ P_t \in [P_2, P_3]\},$$
$$[P_1{}^-, P_2, P_3] := \{P \in \overline{\mathcal{H}} \mid P \in [P_t, P_1] \ \text{ for } \ P_t \in [P_2, P_3]\}.$$

$$[P_1{}^-, P_2, P_3] \qquad\qquad\qquad [P_1{}^+, P_2, P_3]$$
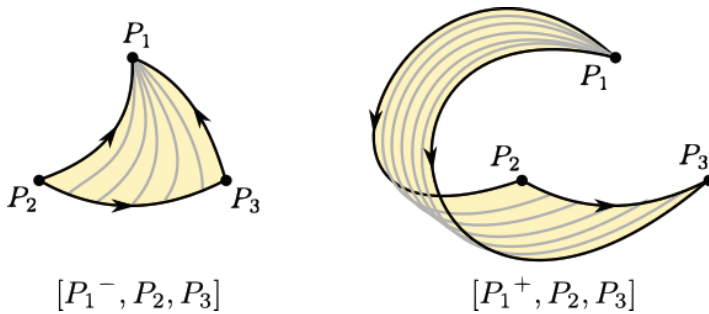
FIGURE 6. *Marked triangles are foliated by oriented edge.*

By fixing P_1 to be at infinity, a marked triangle is half a cylinder with base part of a finite $\mathbb{C}$–circle. One of the advantages of using marked triangles is that they are uniquely determined by their vertices. The following result is a direct consequence of Lemma 7.

LEMMA 9.   *Let P_1, P_2, P_3 and Q_1, Q_2, Q_3 be two triples of points of $\overline{\mathcal{H}}$ in general position. Suppose there exists $G \in \mathrm{PU}(2,1)$ such that $G(P_j) = Q_j$, for all $j \in \{1, 2, 3\}$. Then*

$$G([P_1{}^\star, P_2, P_3]) = [Q_1{}^\star, Q_2, Q_3], \qquad \star \in \{+, -\}.$$

4.3. CR Tetrahedra and Slabs. Given four points of $\overline{\mathcal{H}}$ in general position, a choice of a marked triangle for each triple will not always patch up to form the boundary of a 3–simplex. On one hand, adjacent faces need to agree on the choice of $\mathbb{C}$–circle between the common vertices to have well defined edges. On the other hand,

they could intersect away from the edges. One quickly finds that there is no canonical choice of marked triangles which always works, thus three dimensional simplices need to be checked on a case by case basis.

Here we are going to describe two fundamental 3–cells, which will be the building blocks of the CR structures in §5. They are subsets of the Heisenberg space, both homeomorphic to the closed 3–ball, but equipped with different simplicial structures and thus combinatorially different. These spaces are defined to be especially symmetric, in the sense that several of their faces can be glued pairwise with monotone maps (cf. Lemma 11). That is not always the case for generic triangles, as previously underlined in Lemma 8.

The standard symmetric tetrahedron. Let ω be the cube root of unity $\omega = -\frac{1}{2}\left(1 + i\sqrt{3}\right)$. We consider the following 4–tuple of points in general position in Heisenberg space:

$$P_1 := (1, \sqrt{3}), \qquad P_2 := (-\omega, \sqrt{3}), \qquad P_3 := (0, 0), \qquad P_4 := \infty.$$

For each triple of points, we consider the following marked triangles:

(1) $[P_4^-, P_1, P_2]$: the oriented segment $[P_1, P_2]$ is the shortest arc of the circle $(e^{i\theta}, \sqrt{3})$, oriented from P_1 to P_2. The triangle $[P_4^-, P_1, P_2]$ is part of a cylinder, foliated by vertical segments above $[P_1, P_2]$.

(2) $[P_4^-, P_3, P_1]$: the edge $[P_3, P_1]$ is an arc of ellipse which projects onto the z–coordinate of the Heisenberg space as an arc of the unit circle with centre $-\omega$. It is given by the parametrisation

$$[P_3, P_1] := \left(-\omega + e^{is}, \sqrt{3}\cos(s) - \sin(s)\right), \qquad s : -\frac{2\pi}{3} \mapsto -\frac{\pi}{3}.$$

Hence $[P_4^-, P_3, P_1]$ is foliated by the vertical rays from $[P_3, P_1]$ to P_4.

(3) $[P_4^-, P_3, P_2]$: this marked triangle is obtained by a $\frac{\pi}{3}$ clockwise rotation of the previous triangle $[P_4^-, P_3, P_1]$.

(4) $[P_2^-, P_3, P_1]$ and $[P_3^+, P_1, P_2]$: the first marked triangle is foliated by oriented edges from $[P_3, P_1]$ to P_2. For $\varphi(t, s) := t + s + \frac{\pi}{3}$, we have

$$[P_2^-, P_3, P_1] := \left(e^{i\varphi(t,s)} + e^{i(s - \frac{\pi}{3})} - \omega, -\sin(\varphi(t,s)) - \sin(\varphi(t,0))\right.$$

$$\left. + \sin(s) + \sqrt{3}\left(\cos(\varphi(t,s)) - \cos(t,0) + \cos(s) + 1\right)\right),$$

where $s : -\frac{2\pi}{3} \mapsto -\frac{\pi}{3}$ and $t : 0 \mapsto \frac{\pi}{3}$. The latter one instead, is foliated by oriented edges from P_3 to $[P_1, P_2]$. It can be parametrised as

$$[P_3^+, P_1, P_2] := \left(e^{it}\left(-\omega + e^{is}\right), \sqrt{3}\cos(s) - \sin(s)\right),$$

$$s : -\frac{2\pi}{3} \mapsto -\frac{\pi}{3}, \quad t : 0 \mapsto \frac{\pi}{3}.$$

LEMMA 10. *([8]) The spaces*

$$[P_4^-, P_1, P_2] \cup [P_4^-, P_3, P_1] \cup [P_4^-, P_3, P_2] \cup [P_2^-, P_3, P_1], \tag{1}$$

$$[P_4^-, P_1, P_2] \cup [P_4^-, P_3, P_1] \cup [P_4^-, P_3, P_2] \cup [P_3^+, P_1, P_2], \tag{2}$$

are combinatorially isomorphic to the boundary of a 3–simplex. In particular, they bound a 3–ball on each side in $\overline{\mathcal{H}}$.

The *standard (symmetric) tetrahedron* $\mathfrak{T}_A$ of type *A* (resp. *type B*) is (the closure of) the 3–ball bounded by (1) (resp. by (2) which is contained in the upper half of $\overline{\mathcal{H}}$. Figure 7 shows $\mathfrak{T}_A$ and $\mathfrak{T}_B$ in the Heisenberg model.
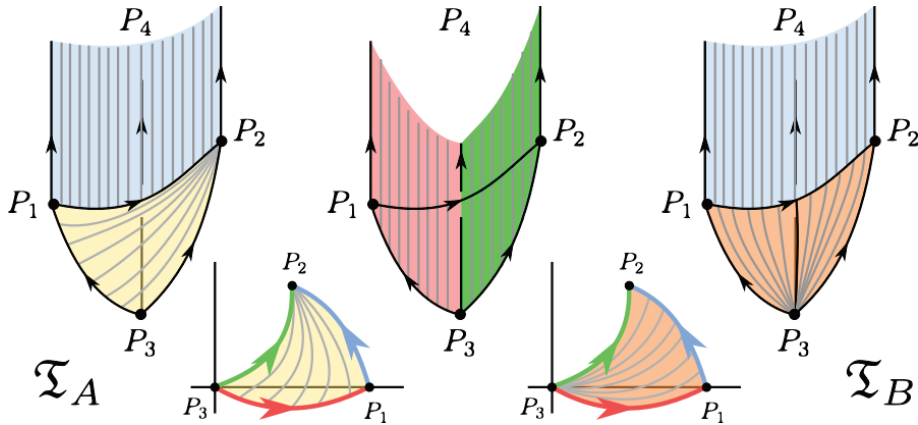

FIGURE 7. *The standard symmetric tetrahedra $\mathfrak{T}_A$ and $\mathfrak{T}_B$ only differ along the face with vertices* $\{P_1, P_2, P_3\}$. *Their standard embeddings in Heisenberg space and their $\mathbb{C}$–projections are displayed here.*

These tetrahedra exhibit various symmetries, for example an anti-holomorphic involution swapping the vertices P_1 with P_2, and P_3 with P_4 (cf. [29]). Furthermore, the vertices of each face (taken with the correct cyclic order) have the same Cartan angle,

$$\mathring{A}(P_2, P_3, P_1) = \mathring{A}(P_4, P_1, P_2) = \mathring{A}(P_4, P_3, P_2) = \mathring{A}(P_4, P_3, P_1) = \frac{\pi}{3}.$$

As a consequence of Lemma 8 and Lemma 9, we can glue faces of $\mathfrak{T}_A$ and $\mathfrak{T}_B$ pairwise by (unique) CR transformations. Consider the following matrices of $PU(2,1)$,

$$G_1 := \begin{bmatrix} -\omega & 0 & 0 \\ 1 & 1 & 0 \\ -\overline{\omega} & \omega & -\omega \end{bmatrix}, \qquad G_2 := \begin{bmatrix} 1 & 1 & \omega \\ 0 & -\overline{\omega} & \overline{\omega} \\ 0 & 0 & 1 \end{bmatrix}, \qquad G_3 := \begin{bmatrix} 1 & 0 & 0 \\ 0 & -\omega & 0 \\ 0 & 0 & 1 \end{bmatrix}.$$

These are the unique CR transformations mapping:

$G_1: \quad P_4 \mapsto P_2 \quad P_3 \mapsto P_3 \quad P_1 \mapsto P_1 \quad$ hence $\quad [P_4^-, P_3, P_1] \mapsto [P_2^-, P_3, P_1],$

$G_2: \quad P_4 \mapsto P_4 \quad P_1 \mapsto P_3 \quad P_2 \mapsto P_2 \quad$ hence $\quad [P_4^-, P_1, P_2] \mapsto [P_4^-, P_3, P_2],$

$G_3: \quad P_4 \mapsto P_4 \quad P_3 \mapsto P_3 \quad P_1 \mapsto P_2 \quad$ hence $\quad [P_4^-, P_3, P_1] \mapsto [P_4^-, P_3, P_2].$

We remark that G_2 and G_3 are face pairings between two standard tetrahedra of any types, while G_1 necessarily glues onto a face of the standard tetrahedron of type *A*. Furthermore, G_2 and G_3 can be described quite nicely in Heisenberg coordinates:

$$G_2([z, t]) = \left[-\overline{\omega}(z - 1) , \ \sqrt{3}\overline{\omega}(z + \overline{\omega} - 1)(z + \omega) + t \right],$$

$$G_3([z, t]) = [-\omega z , \ t].$$

The transformation G_2 preserves vertical $\mathbb{C}$–circles and it restricts on the z–plane to a $\frac{\pi}{3}$ clockwise rotation around the point $-\omega$. The transformation G_3 is a $\frac{\pi}{3}$ anticlockwise rotation of $\overline{\mathcal{H}}$ around the vertical $\mathbb{C}$–circle through $[0, 0]$.

The slabs. The next fundamental piece that we are going to define is of the combinatorial type of the CW complex obtained by deformation retracting the base of a square pyramid onto one of its sides (Figure 8). In particular, it is a 3–cell bounded by two triangular faces and two bigons. It contains a total of five 1–cells and three 0–cells.
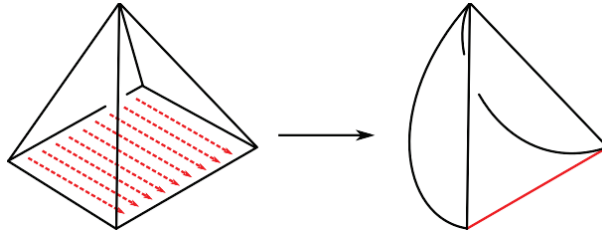

FIGURE 8. *A slab is obtained by deformation retracting the base of a square pyramid onto one of its sides.*

We define the following bigons of $\overline{\mathcal{H}}$:

$$B' := \left(1 + te^{-i\frac{\pi}{6}}, s\right), \qquad t \in \mathbb{R}_{>0} \cup \{\infty\}, \quad s \in \mathbb{R} \cup \{\infty\},$$

$$B_k := \left(-\omega + te^{i\frac{\pi}{6}(1-2k)}, s\right), \qquad t \in \mathbb{R}_{>0} \cup \{\infty\}, \quad s \in \mathbb{R} \cup \{\infty\}, \quad k \in \mathbb{Z}.$$

We remark that both B' and B_k are foliated by vertical $\mathbb{C}$–circles. In particular, $B' \cap B_k = \infty$ for all k. Moreover,

$$B_{k_1} = B_{k_2} \iff k_1 = k_2 \mod 6.$$

The CW complex obtained by attaching

$$[P_4{}^+, P_1, P_2] \; \cup \; [P_4{}^-, P_1, P_2] \; \cup \; B' \; \cup \; B_k,$$

is topologically a 2–sphere. For all k, it bounds a 3–ball containing the point $(2, \sqrt{3}) \in \overline{\mathcal{H}}$. We define the *slab* $\mathfrak{S}_k$ to be (the closure of) such 3–ball. The slabs $\mathfrak{S}_{k_1}$ and $\mathfrak{S}_{k_2}$ are geometrically equivalent if and only if $k_1 = k_2 \mod 6$, in the sense that there is $G \in \mathrm{PU}(2,1)$ such that $G(\mathfrak{S}_{k_1}) = \mathfrak{S}_{k_2}$. This is due to the fact that the 2–skeletons of $\mathfrak{S}_{k_1}$ and $\mathfrak{S}_{k_2}$ only differ along one face. Whence we defined a total of six different slabs. Two examples $\mathfrak{S}_1$ and $\mathfrak{S}_4$ are depicted in Figure 9.

As we mentioned earlier, $\mathring{A}(P_4, P_1, P_2) = \mathring{A}(P_3, P_1, P_2)$, hence let G_4 be the (unique) element of $\mathrm{PU}(2,1)$:

$$G_4 := \begin{bmatrix} 0 & 0 & -\omega \\ 0 & -\overline{\omega} & 0 \\ -\omega & 0 & 1 - \overline{\omega} \end{bmatrix}, \qquad \begin{aligned} & G_4 : P_4 \mapsto P_3 \quad P_1 \mapsto P_1 \quad P_2 \mapsto P_2, \\ & \qquad [P_4{}^+, P_1, P_2] \mapsto [P_3{}^+, P_1, P_2]. \end{aligned}$$

For all k, the CR transformation G_4 is a face pairing between the slab $\mathfrak{S}_k$ and the standard tetrahedron of type B.

The use of six different slabs turns out to be necessary in the general construction of §5.3. The reason for the number six is due to the fact that the CR transformations
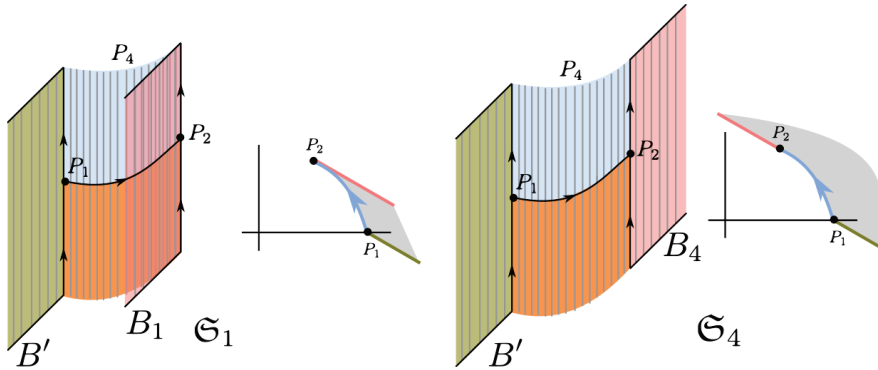
FIGURE 9. *Standard embeddings in Heisenberg space and $\mathbb{C}$–projections of the slabs $\mathfrak{S}_1$ and $\mathfrak{S}_4$.*

G_1, G_2, G_3 and G_4 are all of order six. The connection between these transformations and the slabs is revealed in Theorem 18.

We conclude this section with a definition and an observation. Let W_1 and W_2 be two CW complexes embedded in $\overline{\mathcal{H}}$, and let $G \in \mathrm{PU}(2,1)$ be a face pairing between the faces $F_1 \subset W_1$ and $F_2 \subset W_2$. Then $G(W_1)$ and W_2 might intersect away from $G(F_1) = F_2$. We say that the face pairing G is *monotone* if there are neighbourhoods $\mathcal{N}_1, \mathcal{N}_2$ of F_1, F_2 in W_1, W_2 respectively such that $\mathcal{N}_2 \cap G(W_1) = G(\mathcal{N}_1) \cap W_2 = F_2$. Monotonicity will play an important role in §5 to ensure that the developing maps are locally injective at the faces. The issue we want to avoid here is for W_2 to be glued to W_1 on the "wrong" side of the common face. The following result generalises an observation by Falbel [8].

LEMMA 11. *The transformations G_1, G_2, G_3 are monotone face pairings of the standard symmetric tetrahedra $\mathfrak{T}_A$ and $\mathfrak{T}_B$, while G_4 is a monotone face pairing between the slab and the standard tetrahedron of type B.*

Proof. The transformations G_2 and G_3 are simple to check. They preserve vertical $\mathbb{C}$–circles, therefore one only needs to check the intersection of the projections of the tetrahedra on the z–plane.

On the other hand, G_1 and G_4 are more tedious. We give a summary of the argument for G_4, and refer to [8, Section 6.4] for G_1. Consider the slab $\mathfrak{S}_k$ and the tetrahedron $\mathfrak{T}_B$. The transformation G_4^{-1} glues $\mathfrak{T}_B$ to $\mathfrak{S}_k$ along the face $[P_4^+, P_1, P_2] = G_4^{-1}([P_3^+, P_1, P_2])$. The remaining vertex of $\mathfrak{T}_B$ is mapped to the point $G_4^{-1}(P_4) = [0, 2\sqrt{3}]$ in Heisenberg space. The projection of the 1–skeleton of $G_4^{-1}(\mathfrak{T}_B)$ is displayed next to the projection of $\mathfrak{S}_1$ in Figure 10.

Let R be the region of $\mathbb{C}$–plane bounded by the straight segment from 0 to 1, and the projections of the edges $[P_1, P_2]$ and $G_4^{-1}([P_4, P_2])$. Then $G_4^{-1}(\mathfrak{T}_B)$ is completely contained in the vertical cylinder of Heisenberg space with base R. In particular, there is a neighbourhood of the common face where $G_4^{-1}(\mathfrak{T}_B)$ and $\mathfrak{S}_k$ only intersect along the face, and therefore G_4^{-1} is a monotone face pairing between $\mathfrak{S}_k$ and $\mathfrak{T}_B$. By symmetry of the definition, we conclude that G_4 is also monotone. $\square$

5. Branched CR structures on once-punctured torus bundles. Let M_f be a hyperbolic once-punctured torus bundle. In this section we prove the main result of this paper, that M_f admits a branched CR structure (cf. Theorem 18). We start by formalising the notion of a branched CR structure on M_f. Definitions and
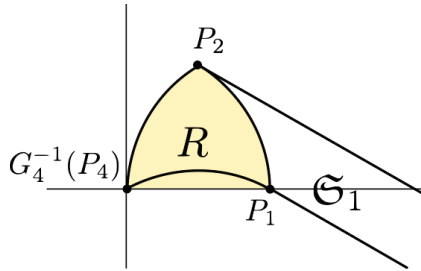
FIGURE 10. *The projection of the 1–skeleton of $G_4^{-1}(\mathfrak{T}_B)$ next to the projection of $\mathfrak{S}_1$.*

terminology are inspired by the work on branched analytic structures on Riemann surfaces in [20]. Then we describe CR structures as tame geometric realizations of ideal decompositions. Finally, we give the construction for the figure eight knot §5.2 and in the general case §5.3.

A *branched covering* between two manifolds is a covering map everywhere except for a nowhere-dense set, called the *branch locus*. For example, the *standard CR branching map* $\xi : \overline{\mathcal{H}} \to \overline{\mathcal{H}}$ defined by $\xi(z,t) := (z^N, t)$ is a branched cyclic covering of ramification order $N \in \mathbb{N} \setminus \{0\}$. In particular, ξ is locally injective everywhere except at the branch locus, namely the Heisenberg t–axis, where the total angle is $2N\pi$. Roughly speaking, branched structures are generalizations of geometric structures where instead of insisting that the charts are local diffeomorphisms, we only require that they are branched covering maps. This construction is quite general, but here we use a very specific instance where M_f has a cell $\mathcal{D}$ decomposition with branched locus a subset of its set of 1–cells $\mathcal{D}^{(1)}$, and charts around the branched locus are all modelled on the standard CR branching map ξ.

More precisely, let $\mathcal{D}$ be a cell decomposition of M_f. A *branched projective chart* $\{U, \phi\}$ of M_f (with respect to $\mathcal{D}$) is an open subset $U \subset M_f$ such that:
- if U is disjoint from $\mathcal{D}^{(1)}$, then $\phi : U \to V$ is a local diffeomorphism into an open subset V of the CR space $\overline{\mathcal{H}}$;
- if $U \cap \mathcal{D}^{(1)} \neq \emptyset$ then ϕ maps the components of $U \cap \mathcal{D}^{(1)}$ diffeomorphically to disjoint segments of $\mathbb{C}$–circles and each $p \in U \cap \mathcal{D}^{(1)}$ has a neighborhood $\mathcal{N}$ on which the restriction of ϕ is a branched cyclic covering of finite order with branch locus $\mathcal{N} \cap \mathcal{D}^{(1)}$.

A *CR branched coordinate covering* of M_f (w.r.t. $\mathcal{D}$) consists of a collection of branched projective charts $\{U_j, \phi_j\}$ where the set $\{U_j\}$ form an open covering of M_f. A *branched CR cover* is a coordinate covering $\{U_j, \phi_j\}$ such that, on each non-empty intersection $U_i \cap U_j$, there are homeomorphisms called *coordinate transition functions*

$$G_{ij} : \phi_i(U_i \cap U_j) \to \phi_j(U_i \cap U_j),$$

that are restrictions of elements in PU(2, 1). In particular they satisfy $G_{ij} \circ \phi_i = \phi_j$. A *branched CR structure* on M_f (w.r.t. $\mathcal{D}$) is an equivalence class of branched CR covers, where two branched CR covers are equivalent if their union is a branched CR cover. To avoid unnecessary repetitions, we are not going to specify that the structure is with respect to a cell decomposition when it is clear from the context.

Let $\{U_j, \phi_j\}$ be a branched CR structure on M_f. When the ramification order of each chart ϕ_j is one, they are homeomorphisms and one recovers the usual definitions

of coordinate covering, CR cover and CR structure [27]. We recall that every CR structure admits a *developing map* and a *holonomy representation*,

$$\mathrm{dev} : \widetilde{M_f} \to \overline{\mathcal{H}} \qquad \text{and} \qquad \mathrm{hol} : \pi_1(M_f) \to \mathrm{PU}(2,1),$$

such that

$$\mathrm{hol}(\gamma) \cdot \mathrm{dev}(x) = \mathrm{dev}(\gamma \cdot x), \qquad \gamma \in \pi_1(M_f), \quad x \in \widetilde{M_f}. \tag{3}$$

The developing map is considered up to deck transformation invariant isotopy, and the pair (dev, hol) is uniquely determined up to the following action of $\mathrm{PU}(2,1)$:

$$G \cdot (\mathrm{dev}, \mathrm{hol}) := (G \cdot \mathrm{dev}, \ G \cdot \mathrm{hol} \cdot G^{-1}), \qquad G \in \mathrm{PU}(2,1).$$

Developing maps thus obtained are locally injective, as the charts ϕ_j are homeomorphisms. Vice versa, a locally injective developing map together with a holonomy representation satisfying the equivariance condition (3), always defines a CR structure. We refer the reader to [28] for a full treatment in the wider context of geometric (G, X)–structures.

In a similar fashion, branched projective structures can be described globally as a pair (dev, hol) where $\mathrm{hol} : \pi_1(M_f) \to \mathrm{PU}(2,1)$ is a representation and $\mathrm{dev} : \widetilde{M_f} \to \overline{\mathcal{H}}$ is a hol–equivariant local diffeomorphism away from the branched locus, and locally a cyclic branched cover of finite order at the branched locus. From the motivational point of view, given only a representation into $\mathrm{PU}(2,1)$, it is not clear that it occurs as the holonomy representation of a spherical CR structure. In that sense, it is useful to consider the more general definition of a branched structure, in the hope that any given representation might be understood in a geometric way. The only difference being that developing maps are not locally injective but locally branched coverings. In particular, the holonomy around each connected component of the branch locus is a rotation by an integer multiple of 2π, and therefore trivial, ensuring a well defined representation of $\pi_1(M_f)$.

5.1. Tame geometric realizations. In §5.3 we construct special branched CR structures on M_f, whose branch locus is a disjoint union of curves. The strategy is to use an *ideal cell decomposition* $\mathcal{D}_f$ of M_f, built using the monodromy ideal triangulation $\mathcal{T}_f$, whose edge set contains the branch locus. We are going to realise each ideal cell as a geometric object in Heisenberg space and each face pairing as an element of $\mathrm{PU}(2,1)$, in a compatible fashion. More precisely, suppose $\mathcal{D}_f$ is made up of the ideal 3–cells σ_i, with face pairings g_j. We recall that a face pairing is called monotone when the paired cells only intersect along the common face in a neighbourhood of such face (cf. end of §4.3). A *geometric realization* $\{\phi_i, G_j\}$ of $\mathcal{D}_f$ in $\overline{\mathcal{H}}$ consists of embeddings $\phi_i : \sigma_i \to \overline{\mathcal{H}}$ and CR transformations $G_j \in \mathrm{PU}(2,1)$, satisfying the following condition: if g_j is the gluing map between the faces F_i and F_k of the ideal 3–cells σ_i and σ_k respectively, then G_j is a monotone CR transformation pairing $\phi_i(F_i)$ and $\phi_k(F_k)$ respecting the combinatorics of $\mathcal{D}_f$. Then we say that ϕ_i and G_j are *geometric realizations* of σ_i and g_j respectively.

A geometric realization differs from a branched CR structure only at the edges. For each edge e, consider a small oriented loop γ_e around e, with arbitrary starting point $x \in \gamma_e$ contained in the interior of some cell. Let $F_0^e \ldots F_{N_e}^e$ be the sequence of faces in $\mathcal{D}_f$ containing e, ordered as they are crossed by γ_e, starting from x. As γ_e travels through a face F_j^e, it leaves an ideal cell σ to enter another ideal cell σ' (possibly equal to σ). Let g_j^e be the face pairing gluing σ to σ' along F_j^e, and let G_j^e

be its corresponding geometric realization. Then the *geometric holonomy* of $\{\phi_i, G_j\}$ along γ_e is the product $\prod_{j=0}^{N_e} G_{N_e-j}^e$. We remark that a different choice of γ_e only changes the geometric holonomy by conjugation or by inverse, hence whether the geometric holonomy around an edge e is trivial (namely equal to the identity) or not, does not depend on the choice of γ_e.

In general, it is not guaranteed that the geometric holonomy of a geometric realization is trivial around an edge. However, when that is the case for every edge of the cell decomposition, then a geometric realization can be extended to a branched CR structure. More precisely, there is a branched CR structure on M_f whose set of charts include the embeddings ϕ_i, and the coordinate transition functions along the faces are the CR transformations G_j. In particular, it is important that the maps G_j are monotone to ensure local injectivity at the faces. Furthermore, the fact that the geometric holonomy around an edge e is trivial allows the construction of a chart containing e which is a branched covering (with branch locus e) and which agrees with ϕ_i around e. An example of this construction in the context of ideal triangulations and real hyperbolic structures can be found in [30].

For future reference, we summarise the above discussion in the following result.

LEMMA 12. *Let $\{\phi_i, G_j\}$ be a geometric realization of $\mathcal{D}_f$ in $\overline{\mathcal{H}}$. If the geometric holonomy around each edge is trivial, then $\{\phi_i, G_j\}$ defines a branched CR structure on M_f.*

In a similar fashion to ideal triangulations, the ideal cell decomposition $\mathcal{D}_f$ we are going to construct is the complement of the 0–skeleton of a CW complex, which is also called $\mathcal{D}_f$. This CW complex is topologically homeomorphic to the *end-compactification* of M_f. It has a single vertex, which is the only non-manifold point. When talking about (ideal) cells in $\mathcal{D}_f$, it will be convenient to consider the 0–skeleton as a point of reference, but we will not always underline that it is not actually part of the decomposition of M_f. Moreover, we are often going to drop the word "ideal" when it is clear from the context.

Since an ideal 3–cell is not compact, embeddings can be complicated in a neighbourhood of an ideal vertex. A *tame geometric realization* of $\mathcal{D}_f$ in $\overline{\mathcal{H}}$ is a geometric realization $\{\phi_i, G_j\}$ whose embeddings $\phi_i : \sigma_i \to \overline{\mathcal{H}}$ extend to the 0–skeleton. Tame geometric realizations are slightly easier to deal with, as we can use the image of the 0–skeleton as reference points for the cells. Let $\widetilde{\mathcal{D}_f}$ be the ideal cell decomposition of the universal cover $\widetilde{M_f}$ induced by $\mathcal{D}_f$. If $\{\phi_i, G_j\}$ is a tame geometric realization with trivial geometric holonomy around each edge, then it defines a branched CR structure, represented by some pair (dev, hol) of developing map and holonomy representation. By tameness, the developing map dev $: \widetilde{\mathcal{D}_f} \to \overline{\mathcal{H}}$ extends equivariantly to the 0–skeleton $\widetilde{\mathcal{D}_f}^{(0)}$. More precisely, if $\mathrm{dev}^{(0)}$ is the restriction of dev to $\widetilde{\mathcal{D}_f}^{(0)}$, then

$$\mathrm{hol}(\gamma) \cdot \mathrm{dev}^{(0)}(x) = \mathrm{dev}^{(0)}(\gamma \cdot x), \qquad \gamma \in \pi_1(M_f), \quad x \in \widetilde{\mathcal{D}_f}^{(0)}.$$

5.2. The figure eight knot complement. The *figure eight knot complement* K_8 is the 3–manifolds obtained by removing a closed tubular neighbourhood of the figure eight knot from the three-sphere. Topologically, it is homeomorphic to the once-punctured torus bundle associated to the flip sequence $\mathbf{w}_8 = \mathcal{RL}$. The corresponding monodromy ideal triangulation $\mathcal{T}_8$ has two tetrahedra: $\sigma_0^{\mathcal{R}}$ of type $\mathcal{R}$ and $\sigma_1^{\mathcal{L}}$ of type $\mathcal{L}$ (see Figure 11). As a cyclic word, $\mathbf{w}_8$ has a subsequence $\mathcal{LRL}$ and

a subsequence $\mathcal{RLR}$, corresponding to the two edges $e_\mathcal{R}$ and $e_\mathcal{L}$ of $\mathcal{T}_8$ respectively (cf. Lemma 5). Both edges have valence six. The ribbon of tetrahedra around $e_\mathcal{R}$ is $\sigma_0^\mathcal{R}, \sigma_1^\mathcal{L}, \sigma_0^\mathcal{R}, \sigma_1^\mathcal{L}, \sigma_0^\mathcal{R}, \sigma_1^\mathcal{L}$, as depicted in Figure 12.
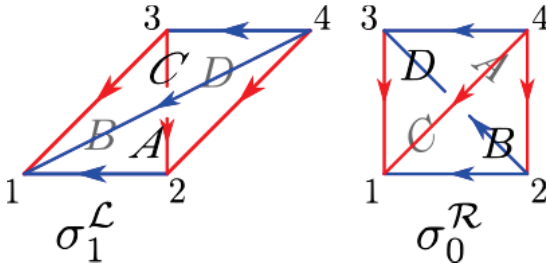

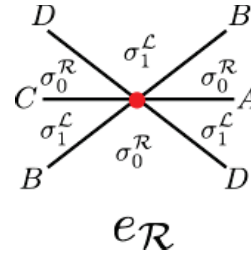FIGURE 11. *The monodromy ideal triangulation of the figure eight knot complement K_8.*

FIGURE 12. *The ribbon of tetrahedra around the red edge $e_\mathcal{R}$, viewed from the vertex $\sigma_0^\mathcal{R}(4)$.*

Now we construct a branched CR structure on K_8, as a preliminary example for the general case in §5.3. The structure we are going to describe here was first discovered by Falbel [8].

Let $\mathcal{D}_8$ be the cell decomposition obtained from the following manipulations on the triangulation $\mathcal{T}_8$.

(1) (Figure 13) We subdivide the face $\sigma_0^\mathcal{R}(134)$ of the tetrahedron $\sigma_0^\mathcal{R}$ into two 2–cells, by introducing a 1–cell with endpoints $\{\sigma_0^\mathcal{R}(1), \sigma_0^\mathcal{R}(4)\}$. The two 2–cells thus obtained are combinatorially a triangle and a bigon. Similarly, we subdivide $\sigma_0^\mathcal{R}(234)$ by placing a 1–cell with endpoints $\{\sigma_0^\mathcal{R}(2), \sigma_0^\mathcal{R}(4)\}$. Finally, we split the tetrahedron $\sigma_0^\mathcal{R}$ into two 3–cells, by introducing a triangular 2–cell with endpoints $\{\sigma_0^\mathcal{R}(1), \sigma_0^\mathcal{R}(2), \sigma_0^\mathcal{R}(4)\}$. Whence $\sigma_0^\mathcal{R}$ is subdivided into two 3–cells: $\hat{\sigma}_0^\mathcal{R}$ with vertices $\{\hat{\sigma}_0^\mathcal{R}(1), \hat{\sigma}_0^\mathcal{R}(2), \hat{\sigma}_0^\mathcal{R}(3), \hat{\sigma}_0^\mathcal{R}(4)\}$ is combinatorially isomorphic to a simplex, and $\hat{\sigma}_0^S$ with vertices $\{\hat{\sigma}_0^S(1), \hat{\sigma}_0^S(2), \hat{\sigma}_0^S(4)\}$ is of the combinatorial type of a slab (cf. §4.3).

(2) (Figure 14) Similar to above, we subdivide $\sigma_1^\mathcal{L}$ into two 3–cells by introducing a 2–cell inside the tetrahedron bounded by two 1–cells with endpoints $\{\sigma_1^\mathcal{L}(2), \sigma_1^\mathcal{L}(4)\}$. Such 1–cells are embedded in the faces $\sigma_1^\mathcal{L}(124)$ and $\sigma_1^\mathcal{L}(234)$ respectively. Thus $\sigma_1^\mathcal{L}$ is decomposed into two 3–cells $\hat{\sigma}_1^\mathcal{L} \cup \hat{\sigma}_1^W$. The former, $\hat{\sigma}_1^\mathcal{L}$ has four triangular faces and a bigon. The latter $\hat{\sigma}_1^W$ is of the combinatorial type of a *wedge*, the CW complex obtained by quotienting a face of a 3–simplex to a point. Its set of vertices is $\{\hat{\sigma}_0^W(2), \hat{\sigma}_0^W(4)\}$.

(3) (Figure 14) We deformation retract the wedge $\hat{\sigma}_1^W$ onto the bigonal face bounded by the red and the black edge. Simultaneously, we collapse the bigonal face of $\hat{\sigma}_1^\mathcal{L}$ into the black edge, transforming $\hat{\sigma}_1^\mathcal{L}$ back into a 3–simplex. Finally, we remove the retracted wedge from the decomposition. As a consequence, the green edge and the black edge of $\hat{\sigma}_0^S$ are now identified (cf. Figure 13 and Figure 15).

A few remarks are in order. Up to step (2), the subdivisions of $\sigma_0^\mathcal{R}$ and $\sigma_1^\mathcal{L}$ agree along the faces, hence they form a well defined cell decomposition of $\mathcal{T}_8$. The importance of this step relies on the fact that the new cell decomposition has more edges than $\mathcal{T}_8$, hence a larger set where we can possibly branch on. On step (3), we flatten the 3–cell $\hat{\sigma}_1^W$ and remove it. This does not change the topology of the complex because a neighbourhood of the red edge $e_\mathcal{R}$ contains other 3–cells other than $\hat{\sigma}_1^W$. In the end we have three 3–cells $\hat{\sigma}_0^\mathcal{R}, \hat{\sigma}_0^S, \hat{\sigma}_1^\mathcal{L}$, two of which are of the combinatorial
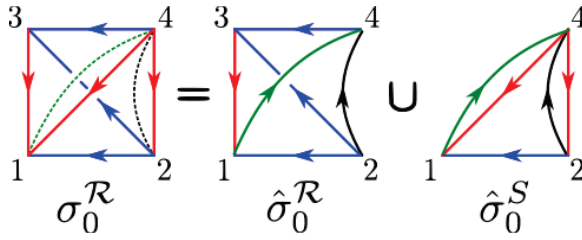
FIGURE 13. *The tetrahedron $\sigma_0^{\mathcal{R}}$ is subdivided into two 3–dimensional cells, of the combinatorial type of a tetrahedron $\hat{\sigma}_0^{\mathcal{R}}$ and a slab $\hat{\sigma}_0^S$.*
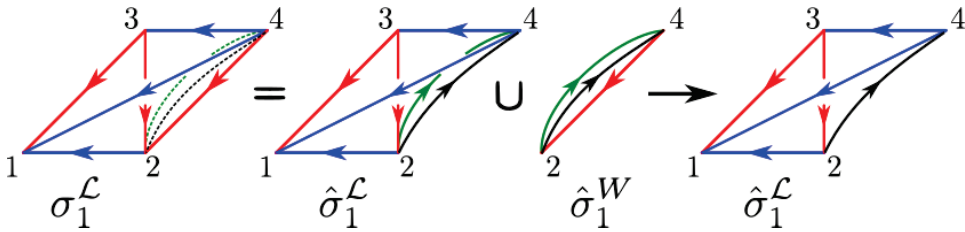

FIGURE 14. *The tetrahedron $\sigma_1^{\mathcal{L}}$ is decomposed into two 3–cells, one of wich is a wedge $\hat{\sigma}_1^W$. The wedge is collapse and removed, while the other 3–cell is deformed back into a tetrahedron $\hat{\sigma}_1^{\mathcal{L}}$.*
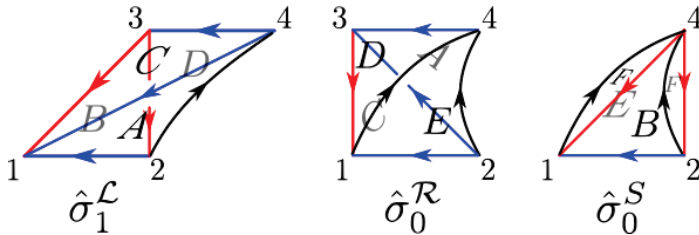

FIGURE 15. *The cell decomposition $\mathcal{D}_8$ of the figure eight knot complement K_8.*

type of a tetrahedron and one of which is a slab (see Figure 15). They glue to form a CW complex $\mathcal{D}_8$, which is a cell decomposition of K_8. Step (3) is crucial because, by removing the wedge $\hat{\sigma}_1^W$ from the decomposition, we avoid the problem of having to geometrically realise it in CR space by an embedding. We remark that in [8], Falbel develops this wedge into a flat bigon. Finally, introducing a slab will allow us to construct a branched CR structure on K_8, and generalize to other manifolds later, however we do not know yet if they are necessary, namely if every CR structure requires at least one.

The slab $\hat{\sigma}_0^S$ has two bigonal faces, with endpoints $\{\hat{\sigma}_0^S(1), \hat{\sigma}_0^S(2)\}$ and $\{\hat{\sigma}_0^S(2), \hat{\sigma}_0^S(4)\}$. Since it would be ambiguous to refer to the edges of $\hat{\sigma}_0^S$ by their vertices, we fix the convention that $\hat{\sigma}_0^S(14)$ and $\hat{\sigma}_0^S(24)$ are the edges belonging to the face shared with $\hat{\sigma}_0^{\mathcal{R}}$, while $\hat{\sigma}_0^S(41)$ and $\hat{\sigma}_0^S(42)$ are the others. These choices were suggested by the embeddings defined in the following paragraph.

We consider the following tame geometric realization of $\mathcal{D}_8$ in $\overline{\mathcal{H}}$. Let $\mathfrak{T}_A, \mathfrak{T}_B$ and $\mathfrak{S}_k$ be the two standard symmetric tetrahedra and the slab defined in §4.3. The

geometric realizations of the ideal cells are the combinatorial isomorphisms defined by

$$\phi_0^{\mathcal{R}} : \hat{\sigma}_0^{\mathcal{R}} \to \mathfrak{T}_A, \qquad \phi_0^S : \hat{\sigma}_0^S \to \mathfrak{S}_1 \qquad \text{and} \qquad \phi_1^{\mathcal{L}} : \hat{\sigma}_1^{\mathcal{L}} \to \mathfrak{T}_B$$

$$\phi_0^{\mathcal{R}}\left(\hat{\sigma}_0^{\mathcal{R}}(1)\right) := P_1, \qquad \phi_0^S\left(\hat{\sigma}_0^S(1)\right) := P_1, \qquad \phi_1^{\mathcal{L}}\left(\hat{\sigma}_1^{\mathcal{L}}(1)\right) := P_1,$$
$$\phi_0^{\mathcal{R}}\left(\hat{\sigma}_0^{\mathcal{R}}(2)\right) := P_2, \qquad \phi_0^S\left(\hat{\sigma}_0^S(2)\right) := P_2, \qquad \phi_1^{\mathcal{L}}\left(\hat{\sigma}_1^{\mathcal{L}}(2)\right) := P_2,$$
$$\phi_0^{\mathcal{R}}\left(\hat{\sigma}_0^{\mathcal{R}}(3)\right) := P_3, \qquad \phi_0^S\left(\hat{\sigma}_0^S(4)\right) := P_4, \qquad \phi_1^{\mathcal{L}}\left(\hat{\sigma}_1^{\mathcal{L}}(3)\right) := P_3,$$
$$\phi_0^{\mathcal{R}}\left(\hat{\sigma}_0^{\mathcal{R}}(4)\right) := P_4, \qquad\qquad\qquad\qquad \phi_1^{\mathcal{L}}\left(\hat{\sigma}_1^{\mathcal{L}}(4)\right) := P_4.$$

We remark that ϕ_0^S maps the edges $\hat{\sigma}_0^S(14)$ and $\hat{\sigma}_0^S(24)$ to the segments of $\mathbb{C}$–circles going from P_1 and P_2, respectively, to P_4. Similarly, $\hat{\sigma}_0^S(41)$ and $\hat{\sigma}_0^S(42)$ are mapped to the segments of $\mathbb{C}$–circles going from P_4 to P_1 and P_2, respectively.

The geometric realizations of the face pairings depicted in Figure 15 are the matrices G_j defined in §4.3, the identity matrix I and a combination thereof. More precisely,

$$A : \hat{\sigma}_1^{\mathcal{L}}(124) \to \hat{\sigma}_0^{\mathcal{R}}(324) \quad \text{is realised by } G_2 \text{ gluing } \mathfrak{T}_B \text{ to } \mathfrak{T}_A,$$
$$B : \hat{\sigma}_0^S(124) \to \hat{\sigma}_1^{\mathcal{L}}(123) \quad \text{is realised by } G_4 \text{ gluing } \mathfrak{S}_1 \text{ to } \mathfrak{T}_B,$$
$$C : \hat{\sigma}_1^{\mathcal{L}}(134) \to \hat{\sigma}_0^{\mathcal{R}}(132) \quad \text{is realised by } G_1 \text{ gluing } \mathfrak{T}_B \text{ to } \mathfrak{T}_A,$$
$$D : \hat{\sigma}_0^{\mathcal{R}}(134) \to \hat{\sigma}_1^{\mathcal{L}}(234) \quad \text{is realised by } G_3 \text{ gluing } \mathfrak{T}_A \text{ to } \mathfrak{T}_B,$$
$$E : \hat{\sigma}_0^{\mathcal{R}}(124) \to \hat{\sigma}_0^S(124) \quad \text{is realised by } I \text{ gluing } \mathfrak{T}_A \text{ to } \mathfrak{S}_1,$$
$$F : \begin{array}{l} \hat{\sigma}_0^S(14) \to \hat{\sigma}_0^S(24) \\ \hat{\sigma}_0^S(41) \to \hat{\sigma}_0^S(42) \end{array} \quad \text{is realised by } G_2 G_3 \text{ gluing } \mathfrak{S}_1 \text{ to } \mathfrak{S}_1.$$

The product $G_2 G_3$, namely the geometric realization of F, maps the bigonal face B' of $\mathfrak{S}_1$ to its other bigonal face B_1. The combinatorics of $\mathcal{D}_8$ around the red $e_{\mathcal{R}}$, black $e'_{\mathcal{R}}$ and blue $e_{\mathcal{L}}$ edges are displayed in Figure 16. One computes that the geometric holonomies are trivial:

$$e_{\mathcal{R}} : \ (G_2 G_3)^{-1} G_4^{-1} G_3 G_1 G_4 = I, \qquad e'_{\mathcal{R}} : \ G_3 I^{-1} (G_2 G_3)^{-1} I G_2 = I,$$

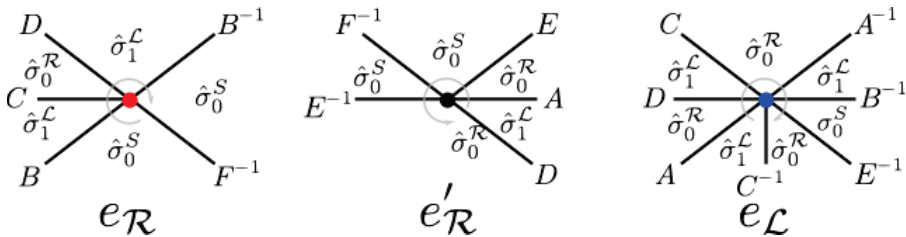$$e_{\mathcal{L}} : \ G_1^{-1} I G_4^{-1} G_2^{-1} G_1 G_3 G_2 = I.$$

FIGURE 16. *The combinatorics around the red $e_{\mathcal{R}}$, black $e'_{\mathcal{R}}$ and blue $e_{\mathcal{L}}$ edges. The view is from the vertices $\hat{\sigma}_0^S(4), \hat{\sigma}_0^{\mathcal{R}}(4)$ and $\hat{\sigma}_0^{\mathcal{L}}(4)$ respectively.*

As per Lemma 12, this tame geometric realization of $\mathcal{D}_8$ in $\overline{\mathcal{H}}$ corresponds to a branched CR structure on K_8 (with respect to $\mathcal{D}_8$). By developing the cells in $\overline{\mathcal{H}}$, one finds that the order of the branching around the edges $e_{\mathcal{R}}$ and $e'_{\mathcal{R}}$ is one, while it is two around $e_{\mathcal{L}}$. These ramification orders were stated incorrectly in [8], and corrected later in [9, Remark 6.1].

5.3. General case. Now we focus on the general case, to show that every hyperbolic once-punctured torus bundle M_f admits a branched CR structure. In particular, we construct an ideal cell decomposition $\mathcal{D}_f$ of M_f, and a tame geometric realization of it in $\overline{\mathcal{H}}$, with trivial geometric holonomy around each edge.

The ideal cell decomposition. Let f be an automorphism of the once punctured torus with two distinct positive real eigenvalues, and let M_f be the corresponding hyperbolic once-punctured torus bundle. Suppose the flip sequence $\mathbf{w}_f$ of M_f has length m. Then the monodromy ideal triangulation $\mathcal{T}_f$ of M_f is made up of m ideal tetrahedra $\sigma_0, \ldots, \sigma_{m-1}$. The ideal cell decomposition $\mathcal{D}_f$ of M_f is obtained from $\mathcal{T}_f$ by performing the three manipulations described in §5.2 to each tetrahedron. We recall from §3.2 that a tetrahedron is said to be of type $\mathcal{R}$ (resp. type $\mathcal{L}$) if the next tetrahedron is layered by a right (resp. left) layering. Thus we modify every tetrahedron of type $\mathcal{R}$ as in step (1), and every tetrahedron of type $\mathcal{L}$ as in (2) and (3). We provide a synthesis of those operations to refresh the notation.

(1) Every tetrahedron $\sigma_j^{\mathcal{R}}$ of type $\mathcal{R}$ is subdivided into two 3–cells, along a newly introduced triangular 2–cell with vertices $\left\{\sigma_j^{\mathcal{R}}(1), \sigma_j^{\mathcal{R}}(2), \sigma_j^{\mathcal{R}}(4)\right\}$. They are a tetrahedron $\hat{\sigma}_j^{\mathcal{R}}$ and a slab $\hat{\sigma}_j^S$.

(2) Every tetrahedron $\sigma_j^{\mathcal{L}}$ of type $\mathcal{L}$ is decomposed into two 3–cells $\hat{\sigma}_j^{\mathcal{L}} \cup \hat{\sigma}_j^W$. The former $\hat{\sigma}_j^{\mathcal{L}}$ has four triangular faces, and a bigon where the wedge $\hat{\sigma}_j^W$ glues to.

(3) We deformation retract the wedge $\hat{\sigma}_j^W$ onto a bigonal face, then remove it. Simultaneously, we collapse the bigonal face of $\hat{\sigma}_j^{\mathcal{L}}$ into one edge, transforming $\hat{\sigma}_j^{\mathcal{L}}$ back into a 3–simplex.

Up to step (2), it is easy to check that the performed subdivisions agree along the faces of $\mathcal{T}_f$, hence they form a well defined cell decomposition of M_f.

Now consider the wedge $\hat{\sigma}_j^W$. We claim that:

CLAIM 13. *Around each of its edges there is always at least one 3–cell that is not a wedge.*

Proof. This is clear for two of its edges, as $\hat{\sigma}_j^W$ glues to the tetrahedron $\hat{\sigma}_j^{\mathcal{L}}$. Call e the remaining edge of $\hat{\sigma}_j^W$. Let $\sigma_j^{\mathcal{L}}$ be the simplex of $\mathcal{T}_f$ from which $\hat{\sigma}_j^W$ is obtained, and let $\sigma_{j+1}^{\star}$ be the next tetrahedron that left layers on top of $\sigma_j^{\mathcal{L}}$. If $\sigma_{j+1}^{\star} = \sigma_{j+1}^{\mathcal{L}}$ is of type $\mathcal{L}$, then $\hat{\sigma}_j^W$ glues to the wedge σ_{j+1}^W around e. On the other hand, if $\sigma_{j+1}^{\star} = \sigma_{j+1}^{\mathcal{R}}$ is of type $\mathcal{R}$, then $\hat{\sigma}_j^W$ glues to the slab σ_{j+1}^S around e. Because f has two distinct real eigenvalues, its flip sequence always contains at least one $\mathcal{R}$ and one $\mathcal{L}$ (cf. §3.1). It follows that around e there is always at least one slab. $\square$

In step (3), we flatten the wedges and remove them. It is a consequence of Claim 13 that this does not change the topology of the complex. Thus in the end we have a CW complex $\mathcal{D}_f$, consisting of three types of 3–cells, two of which are of the combinatorial type of a tetrahedron and one of which is a slab. The complement of the 0–skeleton is an ideal cell decomposition of M_f. We remark that the set of edges of $\mathcal{D}_f$ is larger than the set of edges of $\mathcal{T}_f$, and it contains the branch locus.

Equality holds if and only if the flip sequence $\mathbf{w}_f$ does not contain a subsequence $\mathcal{RLR}$ (cf. Lemma 19,20 and 21).

To avoid introducing new terminology, we are going to make the following abuse of notation. Cells of $\mathcal{D}_f$ coming from tetrahedra of $\mathcal{T}_f$ of type $\mathcal{R}$ (resp. type $\mathcal{L}$) will also be referred to as cells of type $\mathcal{R}$ (resp. type $\mathcal{L}$). Moreover, if a tetrahedron σ_j right layers (resp. left layers) on a tetrahedron σ_{j-1} in $\mathcal{T}_f$, then also the 3–cells of $\mathcal{D}_f$ obtained from σ_j right layer (resp. left layer) on the cells obtained from σ_{j-1}.

Combinatorics around the edges. As mentioned in the example of the figure eight knot complement, a slab $\hat{\sigma}_j^S$ has two bigonal faces, therefore it is ambiguous to refer to its edges by the 0–skeleton. We avoid that by fixing the convention that $\hat{\sigma}_j^S(14)$ and $\hat{\sigma}_j^S(24)$ are the edges belonging to the face shared with the tetrahedron $\hat{\sigma}_j^{\mathcal{R}}$, while $\hat{\sigma}_j^S(41)$ and $\hat{\sigma}_j^S(42)$ are the others. The notation is motivated by the natural orientations of the edges of a geometric slab $\mathfrak{S}_k \subset \overline{\mathcal{H}}$.

Recall that π is the natural quotient map from the disjoint union of the m simplices of $\mathcal{T}_f$ into $\mathcal{T}_f$, defined by the face pairings. Let $\hat{\pi}$ be the corresponding map for $\mathcal{D}_f$. Then the *valence* of an edge in $\mathcal{D}_f$ is the size of its inverse image under $\hat{\pi}$.

THEOREM 14. *Let $\mathcal{D}_f^{(1)}$ be the set of 1–cells in $\mathcal{D}_f$. Let $A \subset \{0,\ldots,m-1\}$ be the subset of indices such that $\hat{\sigma}_j^S$ is a slab of $\mathcal{D}_f$, for all $j \in A$. Then the quotient map $\hat{\pi}$ restricts to a bijection*

$$\hat{\pi}_r : \left\{\hat{\sigma}_j^\star(14)\right\}_{j \in \{0\ldots m-1\}} \cup \left\{\hat{\sigma}_j^S(41)\right\}_{j \in A} \longrightarrow \mathcal{D}_f^{(1)}, \qquad \star \in \{\mathcal{L}, \mathcal{R}\}.$$

Theorem 14 allows us to canonically pick a representative for each edge in $\mathcal{D}_f$. For example, in the case of the figure eight knot complement in §5.2, the chosen representatives are $\hat{\sigma}_1^{\mathcal{L}}(14), \hat{\sigma}_0^{\mathcal{R}}(14)$ and $\hat{\sigma}_0^S(41)$ (respectively the blue, black and red edge in Figure 15). Its proof is a consequence of the following two Lemmas, where we deduce the valence of edges in $\mathcal{D}_f$ from their counterparts in $\mathcal{T}_f$.

LEMMA 15. *Let $\hat{\sigma}_j^{\mathcal{L}}$ be a 3–cell of type $\mathcal{L}$ in $\mathcal{D}_f$, corresponding to a tetrahedron $\sigma_j^{\mathcal{L}}$ in $\mathcal{T}_f$. Let $2n_j + 4$ be the valence of $\pi\left(\sigma_j^{\mathcal{L}}(14)\right)$. Then the equivalence class of $\hat{\sigma}_j^{\mathcal{L}}(14)$ in $\mathcal{D}_f$ is*

$$\left\{\hat{\sigma}_j^{\mathcal{L}}(14), \; \left\{\hat{\sigma}_{j+k}^{\mathcal{R}}(12), \; \sigma_{j+k}^S(12), \; \hat{\sigma}_{j+k}^{\mathcal{R}}(34)\right\}_{k=1,\ldots,n_j}, \right.$$
$$\left. \sigma_{j+n_j+1}^{\mathcal{L}}(12), \; \sigma_{j+n_j+1}^{\mathcal{L}}(34), \; \sigma_{j+n_j+2}^\star(23)\right\},$$

where $\star \in \{\mathcal{L}, \mathcal{R}\}$. In particular $\hat{\pi}\left(\hat{\sigma}_j^{\mathcal{L}}(14)\right)$ has valence $3n_j + 4$.

Proof. By Lemma 5, the edge $\sigma_j^{\mathcal{L}}(14)$ corresponds to a unique subsequence $\mathcal{L}\mathcal{R}^{n_j}\mathcal{L}$ of $\mathbf{w}_f$, for $n_j \geq 0$. In particular, $\sigma_j^{\mathcal{L}}$ is the bottom of a unique ribbon of tetrahedra

$$\sigma_j^{\mathcal{L}} \; \sigma_{j+1}^{\mathcal{R}} \; \cdots \; \sigma_{j+n_j}^{\mathcal{R}} \; \sigma_{j+n_j+1}^{\mathcal{L}} \; \sigma_{j+n_j+2}^\star \; ,$$

where $\star \in \{\mathcal{L}, \mathcal{R}\}$. Whether $\star = \mathcal{L}$ or $\star = \mathcal{R}$ does not depend on the edge $\sigma_j^{\mathcal{L}}(14)$ and does not matter towards the proof of the Lemma. Whence $\sigma_j^{\mathcal{L}}(14)$ is identified with the edges

$$\sigma_j^{\mathcal{L}}(14), \; \left\{\sigma_{j+k}^{\mathcal{R}}(12), \; \sigma_{j+k}^{\mathcal{R}}(34)\right\}_{k=1,\ldots,n_j}, \; \sigma_{j+n_j+1}^{\mathcal{L}}(12), \; \sigma_{j+n_j+1}^{\mathcal{L}}(34), \; \sigma_{j+n_j+2}^\star(23).$$
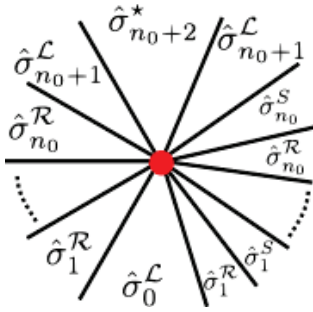
FIGURE 17. *The cross section of a neighbourhood of $\hat{\pi}\left(\hat{\sigma}_0^{\mathcal{L}}(14)\right)$ in $\mathcal{D}_f$, viewed from the vertex $\hat{\sigma}_0^{\mathcal{L}}(4)$.*
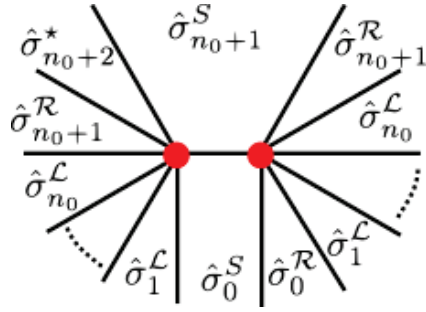
FIGURE 18. *The edge splits into two edges, $\hat{\pi}\left(\hat{\sigma}_0^S(41)\right)$ on the left and $\hat{\pi}\left(\hat{\sigma}_0^S(14)\right)$ on the right. The view is from the vertex $\hat{\sigma}_0^S(4)$*

The valence of its equivalence class in $\mathcal{T}_f$ is $2n_j + 4$. In $\mathcal{D}_f$, we introduce a slab around each edge $\sigma_{j+k}^{\mathcal{R}}(12)$, while neighbourhoods of the other edges glued to e_j are unchanged (cf. Figure 17 for $j = 0$). The statement of the Lemma follows. $\square$

LEMMA 16. *Let $\hat{\sigma}_j^{\mathcal{R}}$ and $\hat{\sigma}_j^S$ be 3–cells of type $\mathcal{R}$ in $\mathcal{D}_f$, corresponding to a tetrahedron $\sigma_j^{\mathcal{R}}$ in $\mathcal{T}_f$. Let $2n_j + 4$ be the valence of $\pi\left(\sigma_j^{\mathcal{R}}(14)\right)$. Then the equivalence class of $\hat{\sigma}_j^{\mathcal{R}}(14)$ in $\mathcal{D}_f$ is*

$$\left\{\hat{\sigma}_j^S(14),\ \hat{\sigma}_j^{\mathcal{R}}(14),\ \left\{\hat{\sigma}_{j+k}^{\mathcal{L}}(24)\right\}_{k=1,\ldots,n_j},\ \hat{\sigma}_{j+n_j+1}^{\mathcal{R}}(24),\ \hat{\sigma}_{j+n_j+1}^S(24)\right\}.$$

Similarly, the equivalence class of $\hat{\sigma}_j^S(41)$ in $\mathcal{D}_f$ is

$$\left\{\hat{\sigma}_j^S(41),\ \left\{\hat{\sigma}_{j+k}^{\mathcal{L}}(13)\right\}_{k=1,\ldots,n_j},\ \hat{\sigma}_{j+n_j+1}^{\mathcal{R}}(42),\ \hat{\sigma}_{j+n_j+2}^{\star}(23),\ \hat{\sigma}_{j+n_j+1}^S(42)\right\},$$

where $\star \in \{\mathcal{L}, \mathcal{R}\}$. In particular, both $\hat{\pi}\left(\hat{\sigma}_j^{\mathcal{R}}(14)\right)$ and $\hat{\pi}\left(\hat{\sigma}_j^S(14)\right)$ have valence $n_j + 4$.

Proof. As in the proof of Lemma 15, the edge $\sigma_j^{\mathcal{R}}(14)$ corresponds to a unique subsequence $\mathcal{R}\mathcal{L}^{n_j}\mathcal{R}$ in $\mathbf{w}_f$, for $n_j \geq 0$. The ribbon of tetrahedra around its edge class in $\mathcal{T}_f$ is

$$\sigma_j^{\mathcal{R}}\ \sigma_{j+1}^{\mathcal{L}}\ \cdots\ \sigma_{j+n_j}^{\mathcal{L}}\ \sigma_{j+n_j+1}^{\mathcal{R}}\ \sigma_{j+n_j+2}^{\star},$$

where $\star \in \{\mathcal{L}, \mathcal{R}\}$. In particular $\sigma_j^{\mathcal{R}}(14)$ is glued to the $2n_j + 4$ edges

$$\sigma_j^{\mathcal{R}}(14),\ \left\{\sigma_{j+k}^{\mathcal{L}}(13),\ \sigma_{j+k}^{\mathcal{L}}(24)\right\}_{k=1,\ldots,n_j},\ \sigma_{j+n_j+1}^{\mathcal{R}}(13),\ \sigma_{j+n_j+1}^{\mathcal{R}}(24),\ \sigma_{j+n_j+2}^{\star}(23).$$

In $\mathcal{D}_f$, the cell $\sigma_j^{\mathcal{R}}(14)$ splits into the bigon with boundary $\hat{\sigma}_j^S(14)$ and $\hat{\sigma}_j^S(41)$. The two loops of the ribbon of tetrahedra around $\sigma_j^{\mathcal{R}}(14)$ in $\mathcal{T}_f$ are split and equidistributed between those two edges in $\mathcal{D}_f$ (cf. Figure 18 for $j = 0$). The statement of the Lemma follows. $\square$

Proof of Theorem 14. First we notice that $\hat{\pi}_r$ is well defined, as it is the restriction of the natural quotient map $\hat{\pi}$. Injectivity follows from Lemma 15 and Lemma 16, because the equivalence classes of $\hat{\sigma}_j^{\mathcal{L}}(14), \hat{\sigma}_j^{\mathcal{R}}(14)$ and $\hat{\sigma}_j^S(41)$ are distinct.

By a topological argument, we deduce that the Euler characteristic of $\mathcal{D}_f$ is zero. Therefore $\mathcal{D}_f$ has as many 3–cells as 1–cells. It follows that $\hat{\pi}_r$ is an injective map between finite sets with the same sizes, thus it is a bijection. $\square$

The tame geometric realization in $\overline{\mathcal{H}}$. A tame geometric realization of $\mathcal{D}_f$ consists of embeddings $\phi_i^{\mathcal{L}}, \phi_i^{\mathcal{R}}, \phi_i^S$ of the 3–cells into $\overline{\mathcal{H}}$, and geometric realizations $G_j \in \mathrm{PU}(2,1)$ of the face pairings.

Let $\hat{\sigma}_j^\star$ be a tetrahedron of $\mathcal{D}_f$, $\star \in \{\mathcal{L}, \mathcal{R}\}$. The development of $\hat{\sigma}_j^\star$ depends on the tetrahedron it layers on. More precisely, let $\hat{\sigma}_{j-1}$ be the tetrahedron in $\mathcal{D}_f$ on top of which $\hat{\sigma}_j^\star$ layers. Then the geometric realization $\phi_j^\star$ of $\hat{\sigma}_j^\star$ is the combinatorial isomorphism

$$\phi_j^\star : \begin{cases} \hat{\sigma}_j^\star \to \mathfrak{T}_B & \text{if } \hat{\sigma}_{j-1} = \hat{\sigma}_{j-1}^{\mathcal{R}} \text{ is of type } \mathcal{R}, \\ \hat{\sigma}_j^\star \to \mathfrak{T}_A & \text{if } \hat{\sigma}_{j-1} = \hat{\sigma}_{j-1}^{\mathcal{L}} \text{ is of type } \mathcal{L}, \end{cases} \quad \text{where} \quad \begin{aligned} \phi_j^\star \left(\hat{\sigma}_j^\star(1) \right) &:= P_1, \\ \phi_j^\star \left(\hat{\sigma}_j^\star(2) \right) &:= P_2, \\ \phi_j^\star \left(\hat{\sigma}_j^\star(3) \right) &:= P_3, \\ \phi_j^\star \left(\hat{\sigma}_j^\star(4) \right) &:= P_4. \end{aligned}$$

Now let $\hat{\sigma}_j^S$ be a slab of $\mathcal{D}_f$. Let $k_j + 4$ be the valence of the edge $\hat{\pi}\left(\hat{\sigma}_j^S(24)\right)$. Then the geometric realization ϕ_j^S of $\hat{\sigma}_j^S$ is the combinatorial isomorphism

$$\phi_j^S : \hat{\sigma}_j^S \to \mathfrak{S}_{k_j} \qquad \text{where} \qquad \begin{aligned} \phi_j^S \left(\hat{\sigma}_j^S(1) \right) &:= P_1, \\ \phi_j^S \left(\hat{\sigma}_j^S(2) \right) &:= P_2, \\ \phi_j^S \left(\hat{\sigma}_j^S(4) \right) &:= P_4. \end{aligned}$$

More precisely, we require that $\phi_j^S \left(\hat{\sigma}_j^S(14) \right) = [P_1, P_4]$ and $\phi_j^S \left(\hat{\sigma}_j^S(24) \right) = [P_2, P_4]$. Thus the bigon with endpoints $\{\hat{\sigma}_j^S(1), \hat{\sigma}_j^S(4)\}$ is developed into

$$B' := \left(1 + t e^{-i\frac{\pi}{6}}, s \right), \qquad t \in \mathbb{R}_{>0} \cup \{\infty\}, \quad s \in \mathbb{R} \cup \{\infty\},$$

while the bigon with endpoints $\{\hat{\sigma}_j^S(2), \hat{\sigma}_j^S(4)\}$ is realised by

$$B_{k_j} := \left(-\omega + t e^{-i\frac{\pi}{6}(1-2k_j)}, s \right), \qquad t \in \mathbb{R}_{>0} \cup \{\infty\}, \quad s \in \mathbb{R} \cup \{\infty\}.$$

Both B' and B_k are foliated by vertical $\mathbb{C}$–circles.

All geometric realizations of the face pairings between triangular faces are uniquely determined by Lemma 8. They are the CR transformations G_i described in §4.3. The remaining ones are either the identity matrix I, or products of the G_i's. We describe them in more detail below.

Let $\hat{\sigma}_j^\star$ be a tetrahedron of $\mathcal{D}_f$, of type $\star \in \{\mathcal{L}, \mathcal{R}\}$. If $\phi_j^\star \left(\hat{\sigma}_j^\star \right) = \mathfrak{T}_A$ is the standard symmetric tetrahedron of type A, then $\hat{\sigma}_j^\star$ layers on a tetrahedron $\hat{\sigma}_{j-1}^{\mathcal{L}}$ of type $\mathcal{L}$. In particular they share two pairs of faces. Let $\mathfrak{T}_X = \phi_{j-1}^{\mathcal{L}} \left(\hat{\sigma}_{j-1}^{\mathcal{L}} \right)$ for some $X \in \{A, B\}$. Then the geometric realizations of the face pairings between $\hat{\sigma}_{j-1}^{\mathcal{L}}$ and $\hat{\sigma}_j^\star$ are:

$$\begin{aligned} \hat{\sigma}_{j-1}^{\mathcal{L}}(134) \to \hat{\sigma}_j^\star(132) \quad &\text{is realised by } G_1 \text{ gluing } \mathfrak{T}_X \text{ to } \mathfrak{T}_A, \\ \hat{\sigma}_{j-1}^{\mathcal{L}}(124) \to \hat{\sigma}_j^\star(324) \quad &\text{is realised by } G_2 \text{ gluing } \mathfrak{T}_X \text{ to } \mathfrak{T}_A. \end{aligned}$$

Now suppose $\phi_j^\star \left(\hat{\sigma}_j^\star \right) = \mathfrak{T}_B$ is the standard symmetric tetrahedron of type B. In this case $\hat{\sigma}_j^\star$ layers on a tetrahedron $\hat{\sigma}_{j-1}^{\mathcal{R}}$ of type $\mathcal{R}$ and on a slab $\hat{\sigma}_{j-1}^S$. Let

$\mathfrak{T}_X = \phi_{j-1}^{\mathcal{R}}\left(\hat{\sigma}_{j-1}^{\mathcal{R}}\right)$, for some $X \in \{A, B\}$, and let $\mathfrak{S}_{k_{j-1}} = \phi_{j-1}^S\left(\hat{\sigma}_{j-1}^S\right)$. Then the geometric realizations of the face pairings between $\hat{\sigma}_{j-1}^{\mathcal{R}}, \hat{\sigma}_{j-1}^S$ and $\hat{\sigma}_j^\star$ are

$$\hat{\sigma}_{j-1}^{\mathcal{R}}(134) \to \hat{\sigma}_j^\star(234) \qquad \text{is realised by } G_3 \text{ gluing } \mathfrak{T}_X \text{ to } \mathfrak{T}_B,$$
$$\hat{\sigma}_{j-1}^{S}(124) \to \hat{\sigma}_j^\star(123) \qquad \text{is realised by } G_4 \text{ gluing } \mathfrak{S}_{k_{j-1}} \text{ to } \mathfrak{T}_B,$$
$$\hat{\sigma}_{j-1}^{\mathcal{R}}(134) \to \hat{\sigma}_{j-1}^S(124) \quad \text{is realised by } I \text{ gluing } \mathfrak{T}_X \text{ to } \mathfrak{S}_{k_{j-1}}.$$

These cover all cases, except for the gluing maps between the bigonal faces of the slabs. Contrary to marked triangles, bigons in Heisenberg space can be identified via many CR transformations. Earlier in this section we showed that around each edge in $\mathcal{D}_f$ there is at most one face pairing gluing two slabs along their bigons (cf. Lemma 15 and Lemma 16). Whence we are going to geometrically realise those face pairings so that the geometric holonomy around each edge is trivial. Under this condition, the choices turn out to be unique.

Consider the slab $\hat{\sigma}_j^S$. By Lemma 16, the equivalence class of the edge $\hat{\sigma}_j^S(14)$ is

$$\left\{\hat{\sigma}_j^S(14), \ \hat{\sigma}_j^{\mathcal{R}}(14), \ \left\{\hat{\sigma}_{j+k}^{\mathcal{L}}(24)\right\}_{k=1,\ldots,n_j}, \ \hat{\sigma}_{j+n_j+1}^{\mathcal{R}}(24), \ \hat{\sigma}_{j+n_j+1}^S(24)\right\}.$$

Let $A_j \ldots, A_{j+n_j+2}$ be the sequence of geometric realizations of the face pairings around $\hat{\pi}\left(\hat{\sigma}_j^S(14)\right)$, starting from $\hat{\sigma}_j^S$ to $\hat{\sigma}_{j+n_j+1}^S$, travelling anticlockwise from the point of view of the vertex $\hat{\sigma}_j^S(4)$. So for example A_j realises the face pairing between $\hat{\sigma}_j^S$ and $\hat{\sigma}_j^{\mathcal{R}}$, while A_{j+n_j+2} corresponds to $\hat{\sigma}_{j+n_j+1}^{\mathcal{R}}$ and $\hat{\sigma}_{j+n_j+1}^S$ (cf. Figure 18 on the right). We remark that $\hat{\sigma}_{j+n_j+1}^S$ is geometrically realised by the slab $\mathfrak{S}_{n_j}$, because the edge $\hat{\pi}\left(\hat{\sigma}_{j+n_j+1}^S(24)\right)$ has valence $n_j + 4$.

LEMMA 17. *The matrix product $\prod_{k=0}^{n_j+2} A_{j+n_j+2-k}$ is a geometric realization of the face pairing between $\hat{\sigma}_j^S$ and $\hat{\sigma}_{j+n_j+1}^S$. In particular, it identifies the bigon B' of $\phi_j^S\left(\hat{\sigma}_j^S\right)$ with the bigon B_{n_j} of $\phi_{j+n_j+1}^S\left(\hat{\sigma}_{j+n_j+1}^S\right)$.*

Proof. By construction, A_j and A_{j+n_j+2} are the identity matrix. On the other hand, $A_{j+1} = G_3$ and $A_{j+k} = G_2$, for all $k \in \{2, \ldots, n_j + 1\}$. Therefore

$$\prod_{k=0}^{n_j+2} A_{j+n_j+2-k} = G_2^{n_j} G_3.$$

We recall from §4.3 that the CR transformations G_3 and G_2 preserve vertical $\mathbb{C}$–circles, and restrict to rotations on the z–plane. In particular, G_3 maps B' to the bigon B_0 and G_2 maps B_k to B_{k+1}. The Lemma follows. $\square$

We remark that the face pairing $\prod_{k=0}^{n_j+2} A_{j+n_j+2-k}$ is monotone, thus this completes the construction of the tame geometric realization of $\mathcal{D}_f$. We conclude the section by showing that these geometric realizations are indeed branched CR structures.

THEOREM 18. *The geometric holonomy around each edge in $\mathcal{D}_f$ is trivial and therefore the geometric realization defines a branched CR structure on M_f.*

Proof. We recall that by Theorem 14 there is a canonical representative for each edge in $\mathcal{D}_f$.

Let $A \subset \{0, \ldots, m-1\}$ be the subset of indexes such that $\hat{\sigma}_j^S$ is a slab of $\mathcal{D}_f$, and let $\overline{A} = \{0, \ldots, m-1\} \setminus A$ be its complement. It is a consequence of Lemma 17 that the geometric holonomy around the edges $\hat{\pi}(\hat{\sigma}_j^{\mathcal{R}}(14))$, for $j \in A$, is trivial.

Consider an edge $\hat{\pi}(\hat{\sigma}_j^S(41))$, for $j \in A$. Let $A_j \ldots, A_{j+n_j+3}$ be the sequence of geometric realizations of all the face pairings around $\hat{\pi}(\hat{\sigma}_j^S(41))$, starting from $\hat{\sigma}_j^S$ and travelling clockwise from the point of view of the vertex $\hat{\sigma}_j^S(4)$ (cf. Figure 18 on the left). Then we have

$$A_j = G_4, \qquad A_{j+k} = G_1 \quad \text{for} \quad k \in \{1, \ldots, n_j\},$$
$$A_{j+n_j+1} = G_3, \qquad A_{j+n_j+2} = G_4^{-1} \qquad A_{j+n_j+3} = G_3 G_2^{-n_j}.$$

Thus the geometric holonomy around $\hat{\pi}(\hat{\sigma}_j^S(41))$ is the product $G_3 G_2^{-n_j} G_4^{-1} G_3 G_1^{n_j} G_4$. Because the matrices G_1 and G_2 are of order six, one only needs to check that the product is the identity matrix for $n_j \in \{0, \ldots, 5\}$. Straight forward computation of the six products gives the result.

An analogous argument works for the edges $\hat{\pi}(\hat{\sigma}_j^{\mathcal{L}}(14))$, $j \in \overline{A}$. The geometric holonomy around them is of the form $G_1^{-1} G_4^{-n_j} G_2^{-1} G_1 G_3^{n_j} G_2$. The matrices G_3 and G_4 are also of order six, hence one only needs to check that the cases $n_j \in \{0, \ldots, 5\}$. The calculation is straightforward.

We apply Lemma 12 to complete the proof. $\square$

6. Properties of the Structures. Consider the branched CR structure on the hyperbolic once-punctured torus bundle M_f described in the previous section 5.3. We conclude by analysing two important features of the structure: the ramification order around each connected component of the branch locus (namely the ideal edges), and the holonomy representation. In §6.1 we show that the ramification order of an edge e has a simple description in terms of the valence of e in the cell decomposition, and therefore its explicitly computable (cf. Theorem 14). In §6.2 we find the holonomy of the generators of $\pi_1(M_f)$ and underline some properties.

6.1. Branch locus. The branch locus of the CR structure of M_f is contained in the union of all ideal edges of the associated cell decompositions $\mathcal{D}_f$. Equality holds if and only if the flip sequence $\mathbf{w}_f$ does not contain a subsequence $\mathcal{RLR}$ (cf. Lemma 19,20 and 21). Here we show that the ramification order around each curve is related to their valence in the simplicial complex. The strategy will be to develop each curve as a vertical line in Heisenberg space, and analyse the projection onto the $\mathbb{C}$–plane of a neighbourhood. This way we can talk about angles of the projections where otherwise it would not be possible. We remind the reader that CR transformations do not preserve angles, therefore the angles we are going to talk about depend on the chosen realizations.

We recall that by Theorem 14 there is a canonical representative for each edge in the cell decomposition $\mathcal{D}_f$, namely $\hat{\sigma}_j^{\mathcal{R}}(14), \hat{\sigma}_j^S(41)$ and $\hat{\sigma}_j^{\mathcal{L}}(14)$. Let ceiling$(x) = \lceil x \rceil$ be the *ceiling function*, which associates x to the smallest integer greater than or equal to x.

LEMMA 19. *Let $n_j + 4$ be the valence of $e_j = \hat{\pi}(\hat{\sigma}_j^{\mathcal{R}}(14))$ in $\mathcal{D}_f$, $n_j \geq 0$. Then the ramification order around e_j is $\left\lceil \frac{n_j+5}{6} \right\rceil$.*

Proof. First, we observe that the geometric realization $\phi_j^{\mathcal{R}}$ develops the edge $\hat{\sigma}_j^{\mathcal{R}}(14)$ into the vertical ray of Heisenberg space going from $P_1 = (1, \sqrt{3})$ to $P_4 = \infty$.
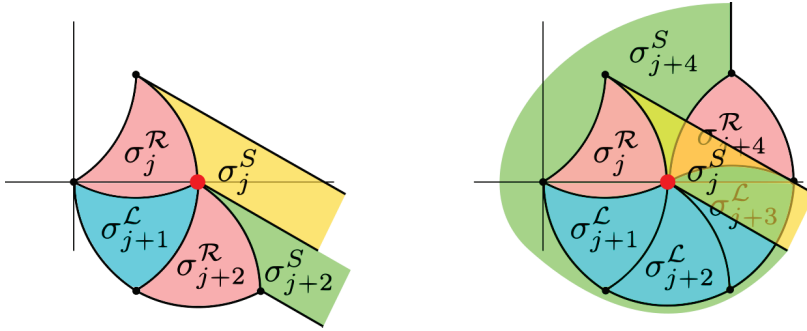
FIGURE 19. *The developments around the branch locus for $n_j = 1$ (on the left) and $n_j = 3$ (on the right). Their respective ramification orders are one and two.*

Therefore we can understand the ramification order of e_j by looking at the projections of the tetrahedra around e_j on the $\mathbb{C}$–plane of $\overline{\mathcal{H}}$.

Let $R \subset \mathbb{C}$ be the projection of the standard symmetric tetrahedron. It is a triangular region bounded by three arcs of circles (cf. Figure 7). We recall from §5.3 (cf. Figure 18) that the sequence of 3–cells around e_j in $\mathcal{D}_f$ is

$$\hat{\sigma}_j^S, \hat{\sigma}_j^\mathcal{R}, \hat{\sigma}_{j+1}^\mathcal{L}, \ldots, \hat{\sigma}_{j+n_j}^\mathcal{L}, \hat{\sigma}_{j+n_j+1}^\mathcal{R}, \hat{\sigma}_{j+n_j+1}^S.$$

Then $\phi_j^\mathcal{R}\left(\hat{\sigma}_j^\mathcal{R}\right)$ projects onto $R_j := R$. The next simplex glues to $\phi_j^\mathcal{R}\left(\hat{\sigma}_j^\mathcal{R}\right)$ via G_3^{-1}, therefore its projection R_{j+1} is a $\frac{\pi}{3}$ clockwise rotation of R_j around the origin. After that, we have n_j simplices each of which is glued to the previous one by G_2^{-1}. Whence each of their projections R_{j+k}, for $k \in \{1, \ldots, n_j + 1\}$, is a $\frac{\pi}{3}$ anticlockwise rotation of R_{k-1} about the point 1. Finally, the projections of the geometric realizations of the two slabs $\hat{\sigma}_j^S, \hat{\sigma}_{j+n_j+1}^S$ rigidly glue to R_j and R_{j+n_j+1} to fill in the gap. Examples for $n_j = 1$ and $n_j = 3$ are depicted in Figure 19.

Around e_j, the first region R_j contributes with an angle of $\frac{2}{3}\pi$, while every other region R_{j+k}, for $k \in \{1, \ldots, n_j + 1\}$, contributes with an angle of $\frac{\pi}{3}$. The first slab also adds $\frac{2}{3}\pi$. This sums up to $\left(\frac{5+n_j}{6}\right) 2\pi$. The angle of the projection of the last slab around e_j is a non-negative number strictly lower than 2π, therefore the total angle is the next integer multiple of 2π. That is $\left\lceil \frac{n_j+5}{6} \right\rceil 2\pi$. □

LEMMA 20. *Let $n_j + 4$ be the valence of $e_j = \hat{\pi}\left(\hat{\sigma}_j^S(41)\right)$ in $\mathcal{D}_f$, $n_j \geq 0$. Then the ramification order around e_j is $\left\lceil \frac{n_j+5}{6} \right\rceil$.*

Proof. This proof is similar to the one of Lemma 19, as the geometric realization ϕ_j^S develops the edge $\hat{\sigma}_j^S(41)$ into the vertical ray from $P_4 = \infty$ to $P_1 = (1, \sqrt{3})$. The only difference is that we are not going to consider the projections of the entire cells, since they are not as clear as in the previous case, but only the projections of the vertices. Every 3–cell around e_j has two vertices at P_4 and P_1, and its angle about e_j is strictly between zero and 2π. Therefore knowing the positions of the other vertices gives us an estimate of the total angle around e_j.

The sequence of 3–cells around e_j in $\mathcal{D}_f$ is

$$\hat{\sigma}_j^S, \hat{\sigma}_{j+1}^\mathcal{L}, \ldots, \hat{\sigma}_{j+n_j}^\mathcal{L}, \hat{\sigma}_{j+n_j+1}^\mathcal{R}, \hat{\sigma}_{j+n_j+2}^\star, \hat{\sigma}_{j+n_j+1}^S,$$

CR face pairing	3–cells	Vertices disjoint from e_j	$\mathbb{C}$–coordinates
G_4	$\hat{\sigma}_j^S$	$\hat{\sigma}_j^S(2)$	$-\omega$
	$\hat{\sigma}_{j+1}^{\mathcal{L}}$	$\hat{\sigma}_{j+1}^{\mathcal{L}}(2)$	$-\omega$
G_1		$\hat{\sigma}_{j+1}^{\mathcal{L}}(4)$	0
G_1	$\hat{\sigma}_{j+1+k}^{\mathcal{L}},$ $k=1,\dots,n_j-1$	$\hat{\sigma}_{j+1+k}^{\mathcal{L}}(2)$	$(-1)^k\omega^{k-1}+1$
		$\hat{\sigma}_{j+1+k}^{\mathcal{L}}(4)$	$(-1)^{k+1}\omega^k+1$
	$\hat{\sigma}_{j+n_j+1}^{\mathcal{R}}$	$\hat{\sigma}_{j+n_j+1}^{\mathcal{R}}(2)$	$(-1)_j^n\omega^{n_j-1}+1$
G_3		$\hat{\sigma}_{j+n_j+1}^{\mathcal{R}}(4)$	$(-1)^{n_j+1}\omega^{n_j}+1$
	$\hat{\sigma}_{j+n_j+2}^{\star}$	$\hat{\sigma}_{j+n_j+2}^{\star}(4)$	$(-1)^{n_j+1}\omega^{n_j}+1$
G_4^{-1}		$\hat{\sigma}_{j+n_j+2}^{\star}(1)$	$(-1)^{n_j+2}\omega^{n_j+1}+1$
	$\hat{\sigma}_{j+n_j+1}^{S}$	$\hat{\sigma}_{j+n_j+1}^{S}(1)$	$(-1)^{n_j+2}\omega^{n_j+1}+1$

TABLE 1. *The list of vertices of the 3–cells around e_j that are not identified with the endpoints of e_j. We recall that $\omega = -\frac{1}{2}\left(1+i\sqrt{3}\right).$*
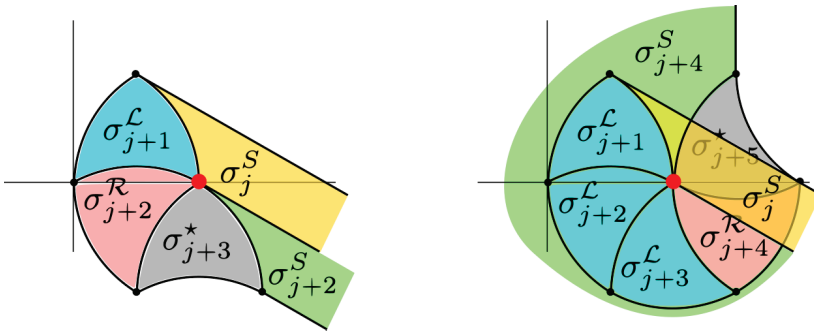

FIGURE 20. *The developments around the branch locus for $n_j = 1$ (on the left) and $n_j = 3$ (on the right). Only vertices and edges are projected. The shaded areas are just guidelines to distinguish the different cells, but they are not the actual projections of the 3–cells. The respective ramification orders are one and two.*

for some $\star \in \{\mathcal{L}, \mathcal{R}\}$. We begin by developing $\phi_j^S\left(\hat{\sigma}_j^S\right)$, then glue every other 3–cell around e_j. The vertices that are not identified with the endpoints of e_j are listed in Table 1. They are all positioned at the vertices of a regular hexagon of edge length $\frac{\sqrt{3}}{2}$.

We draw examples of the projections for $n_j = 1$ and $n_j = 3$ in Figure 20. We remark that these are projections of the vertices and edges, but not of the 2–skeletons as faces are generally not foliated by vertical rays anymore.

Up to $\hat{\sigma}_{j+n_j+2}^{\star}$, the total sum of the angles is strictly between $\left\lceil\frac{n_j-1}{6}\right\rceil$ and $\left\lceil\frac{n_j+5}{6}\right\rceil$. Because the angle of the projection of the last slab around e_j is a non-negative number strictly lower than 2π, the ramification order must be $\left\lceil\frac{n_j+5}{6}\right\rceil$. $\square$

LEMMA 21. *Let $3n_j + 4$ be the valence of $e_j = \hat{\pi}\left(\hat{\sigma}_j^{\mathcal{L}}(14)\right)$ in $\mathcal{D}_f$, $n_j \geq 0$. Then the ramification order around e_j is $n_j + 1$.*

Proof. We follow almost verbatim the proof of Lemma 20.

CR face pairing	3–cells	Vertices disjoint from e_j	$\mathbb{C}$–coordinates
G_1	$\hat{\sigma}_j^{\mathcal{L}}$	$\hat{\sigma}_j^{\mathcal{L}}(2)$	$-\omega$
		$\hat{\sigma}_j^{\mathcal{L}}(3)$	0
I	$\hat{\sigma}_{j+k}^{\mathcal{R}}$ $k=1,\ldots,n_j$	$\hat{\sigma}_{j+k}^{\mathcal{R}}(3)$	$(-1)^k\overline{\omega}^{k-1}+1$
		$\hat{\sigma}_{j+k}^{\mathcal{R}}(4)$	$(-1)^{k+1}\overline{\omega}^k+1$
G_4	$\hat{\sigma}_{j+k}^{S}$, $k=1,\ldots,n_j$	$\hat{\sigma}_{j+k}^{S}(4)$	$(-1)^{k+1}\overline{\omega}^k+1$
G_2	$\hat{\sigma}_{j+n_j+1}^{\mathcal{L}}$	$\hat{\sigma}_{j+n_j+1}^{\mathcal{L}}(3)$	$(-1)^{n_j+1}\overline{\omega}^{n_j}+1$
		$\hat{\sigma}_{j+n_j+1}^{\mathcal{L}}(4)$	$(-1)^{n_j+2}\overline{\omega}^{n_j+1}+1$
	$\hat{\sigma}_{j+n_j+2}^{\star}$	$\hat{\sigma}_{j+n_j+2}^{\star}(4)$	$(-1)^{n_j+2}\overline{\omega}^{n_j+1}+1$
		$\hat{\sigma}_{j+n_j+2}^{\star}(1)$	$(-1)^{n_j+3}\overline{\omega}^{n_j+2}+1$

TABLE 2. *The list of vertices of some of the 3–cells around e_j that are not identified with the endpoints of e_j. We recall that $\omega = -\frac{1}{2}\left(1+i\sqrt{3}\right)$.*

CR face pairing	3–cells	Vertices disjoint from e_j	$\mathbb{C}$–coordinates
G_2	$\hat{\sigma}_j^{\mathcal{L}}$	$\hat{\sigma}_j^{\mathcal{L}}(3)$	0
		$\hat{\sigma}_j^{\mathcal{L}}(2)$	$-\omega$
G_3	$\hat{\sigma}_{j+k}^{\mathcal{R}}$ $k=1,\ldots,n_j$	$\hat{\sigma}_{j+k}^{\mathcal{R}}(2)$	$(-1)^{k+1}\overline{\omega}^k+1$
		$\hat{\sigma}_{j+k}^{\mathcal{R}}(1)$	$(-1)^{k+2}\overline{\omega}^{k+1}+1$
	$\hat{\sigma}_{j+n_j+1}^{\mathcal{L}}$	$\hat{\sigma}_{j+n_j+1}^{\mathcal{L}}(2)$	$(-1)^{n_j+2}\overline{\omega}^{n_j+3}+1$
G_1		$\hat{\sigma}_{j+n_j+1}^{\mathcal{L}}(1)$	$(-1)^{n_j+3}\overline{\omega}^{n_j+2}+1$
	$\hat{\sigma}_{j+n_j+2}^{\star}$	$\hat{\sigma}_{j+n_j+2}^{\star}(1)$	$(-1)^{n_j+3}\overline{\omega}^{n_j+2}+1$
		$\hat{\sigma}_{j+n_j+2}^{\star}(4)$	$(-1)^{n_j+2}\overline{\omega}^{n_j+1}+1$

TABLE 3. *The list of vertices of the remaining 3–cells around e_j that are not identified with the endpoints of e_j.*

First we consider the development $\phi_j^{\mathcal{L}}\left(\hat{\sigma}_j^{\mathcal{L}}\right)$. This geometric realization maps the edge $\hat{\sigma}_j^{\mathcal{L}}(14)$ into the vertical ray from $P_1=(1,\sqrt{3})$ to $P_4=\infty$. From the point of view of the vertex $\hat{\sigma}_j^{\mathcal{L}}(4)$ (cf. Figure 17), starting from $\hat{\sigma}_j^{\mathcal{L}}$ and travelling anticlockwise around e_j until $\sigma_{j+n_j+2}^{\star}$, we encounter the 3–cells

$$\sigma_j^{\mathcal{L}}\ \sigma_{j+1}^{\mathcal{R}}\ \sigma_{j+1}^{S}\ \cdots\ \sigma_{j+n_j}^{\mathcal{R}}\ \sigma_{j+n_j}^{S}\ \sigma_{j+n_j+1}^{\mathcal{L}}\ \sigma_{j+n_j+2}^{\star}.$$

The vertices of these cells that are not identified with the endpoints of e_j are listed in Table 2.

Similarly, if we travel clockwise around e_j, we have

$$\sigma_j^{\mathcal{L}}\ \sigma_{j+1}^{\mathcal{R}}\cdots\ \sigma_{j+n_j}^{\mathcal{R}}\ \sigma_{j+n_j+1}^{\mathcal{L}}\ \sigma_{j+n_j+2}^{\star}.$$

The vertices of these cells that are not identified with the endpoints of e_j are summarised in Table 3.

We remark that for all $k=1,\ldots,n_j$, the 3-cells $\hat{\sigma}_{j+k}^{\mathcal{R}}$ and $\hat{\sigma}_{j+k}^{S}$ cover a total angle of 2π around e_j. When $n_j=0$, the total angle around e_j is exactly of 2π, hence in the general case the ramification order around e_j is n_j+1. $\square$

6.2. The holonomy representation. It was mentioned in §5 that every branched CR structure admits a pair of a developing map and holonomy representation, defined up to the action of $\mathrm{PU}(2,1)$. Let $(\mathrm{dev}_f, \mathrm{hol}_f)$ be a representative pair associated to the branched CR structure on M_f. Here we summarise few facts about hol_f, referring the reader to the author's PhD thesis for more details and the connection to the work of Fock and Goncharov on positive representations [12].

The fundamental group of M_f is an HNN extension of the fundamental group of the base once–punctured torus $\mathbb{T}_0$, namely the free group in two generators $\langle \alpha, \beta \rangle$. It has a standard presentation

$$\pi_1(M_f) = \langle \alpha, \beta, \tau \mid \tau\alpha\tau^{-1} = f_*(\alpha), \ \tau\beta\tau^{-1} = f_*(\beta) \rangle,$$

where $f_* : \langle \alpha, \beta \rangle \to \langle \alpha, \beta \rangle$ is the automorphism induced by f, and τ is represented by the base circle of the fiber bundle. If M_f has flip sequence $\mathbf{w}_f = \mathcal{R}^{a_0}\mathcal{L}^{b_0}\dots\mathcal{R}^{a_k}\mathcal{L}^{b_k}\mathcal{R}^c$ (the other case being similar), there is a choice of the class representative $(\mathrm{dev}_f, \mathrm{hol}_f)$ such that

$$\mathrm{hol}_f(\alpha) = G_4^{-1}G_3, \quad \mathrm{hol}_f(\beta) = G_1^{-1}G_2, \quad \text{and} \quad \mathrm{hol}_f(\tau) = G_4^{-a_0-c}G_1^{-b_0}\dots G_4^{-a_k}G_1^{-b_k}.$$

Let $\rho : \pi_1(\mathbb{T}_0) \to \mathrm{PU}(2,1)$ be the representation obtained by restricting hol_f to $\langle \alpha, \beta \rangle$. Then ρ does not depend on f, namely it is a representation of $\pi_1(\mathbb{T}_0)$ that always extends to a representation of $\pi_1(M_f)$. This is reflected in the fact that the two first building blocks of M_f are always developed in the same way, hence the fiber once-punctured torus also always develops in the same way. We remark that ρ is irreducible, but not strongly irreducible. Moreover, it is not faithful but it has infinite discrete image. In fact, its image $\rho(\pi_1(\mathbb{T}_0))$ is a subgroup of the Eisenstein-Picard modular group $\mathrm{PU}(2,1,\mathbb{Z}[\omega])$, the subgroup of $\mathrm{PU}(2,1)$ with entries in the set of Eisenstein integers $\mathbb{Z}[\omega]$.

The representation ρ was proved to have the above special properties while studying Fock and Goncharov's parametrisation of $\mathfrak{X}^\times(\mathbb{T}_0)$, the decorated $\mathrm{PGL}(3,\mathbb{C})$–character variety of $\mathbb{T}_0$. Using the inclusion map $\overline{\mathcal{H}} \hookrightarrow \mathbb{CP}^2$ together with its first complex jet, one induces a decoration on ρ, making its $\mathrm{PGL}(3,\mathbb{C})$ conjugacy class $[\rho]$ an element of $\mathfrak{X}^\times(\mathbb{T}_0)$. Under this construction, the Fock-Goncharov coordinate of $[\rho]$ is

$$P = (\omega, \omega, \omega, \omega, \omega, \omega, \omega, \omega), \quad \text{where} \quad \omega = -\frac{1}{2}\left(1 + i\sqrt{3}\right).$$

The point P and its complex conjugate are the only points in Fock-Goncharov moduli space that are fixed by every Fock-Goncharov edge flip. Under milder conditions, it should be possible to find other points in Fock-Goncharov moduli space with similar behaviors, perhaps leading to other representations such as ρ, that extend to representations of $\pi_1(M_f)$, and interesting CR structures. More details con be found in the author's PhD thesis [4].

REFERENCES

[1] I. AGOL, *Ideal triangulations of pseudo-Anosov mapping tori*, in "Topology and geometry in dimension three", volume 560 of Contemp. Math., pp. 1–17. Amer. Math. Soc., Providence, RI, 2011.

[2] J. S. BLAND, *Contact geometry and CR structures on S^3*, Acta Math., 172:1 (1994), pp. 1–49.

[3] F. BONAHON, *Low-dimensional geometry*, volume 49 of "Student Mathematical Library". American Mathematical Society, Providence, RI; Institute for Advanced Study (IAS), Princeton, NJ, 2009. From Euclidean surfaces to hyperbolic knots, IAS/Park City Mathematical Subseries.

[4] A. CASELLA, *Branched CR structures on once–punctured torus bundles*, 2018. Thesis (Ph.D.)–University of Sydney, Sydney NSW.

[5] A. CASELLA, F. LUO, AND S. TILLMANN, *Pseudo-developing maps for ideal triangulations II: Positively oriented ideal triangulations of cone-manifolds*, Proc. Amer. Math. Soc., 145:8 (2017), pp. 3543–3560.

[6] J. DANCIGER, *A geometric transition from hyperbolic to anti-de Sitter geometry*, Geom. Topol., 17:5 (2013), pp. 3077–3134.

[7] C. EHRESMANN, *Sur les espaces localement homogènes*, L'ens. Math., 35:1 (1936), pp. 317–335.

[8] E. FALBEL, *A spherical CR structure on the complement of the figure eight knot with discrete holonomy*, J. Differential Geom., 79:1 (2008), pp. 69–110.

[9] E. FALBEL AND J. WANG, *Branched spherical CR structures on the complement of the figure-eight knot*, Michigan Math. J., 63:3 (2014), pp. 635–667.

[10] B. FARB AND D. MARGALIT, *A primer on mapping class groups*, volume 49 of "Princeton Mathematical Series". Princeton University Press, Princeton, NJ, 2012.

[11] W. FLOYD AND A. HATCHER, *Incompressible surfaces in punctured-torus bundles*, Topology Appl., 13:3 (1982), pp. 263–282.

[12] V. FOCK AND A. GONCHAROV, *Moduli spaces of local systems and higher Teichmüller theory*, Publ. Math. Inst. Hautes Études Sci., 1:103 (2006), pp. 1–211.

[13] W. M. GOLDMAN, *Conformally flat manifolds with nilpotent holonomy and the uniformization problem for 3-manifolds*, Trans. Amer. Math. Soc., 278:2 (1983), pp. 573–583.

[14] W. M. GOLDMAN, *Complex hyperbolic geometry*. Oxford Mathematical Monographs. The Clarendon Press, Oxford University Press, New York, 1999. Oxford Science Publications.

[15] F. GUÉRITAUD, *On canonical triangulations of once-punctured torus bundles and two-bridge link complements*, Geom. Topol., 10 (2006), pp. 1239–1284. With an appendix by David Futer.

[16] H. JACOBOWITZ, *An introduction to CR structures*, volume 32 of "Mathematical Surveys and Monographs". American Mathematical Society, Providence, RI, 1990.

[17] Y. KAMISHIMA AND T. TSUBOI, *CR-structures on Seifert manifolds*, Invent. Math., 104:1 (1991), pp. 149–163.

[18] F. KLEIN, *Ueber Liniengeometrie und metrische Geometrie*, Math. Ann., 5:2 (1872), pp. 257–277.

[19] M. LACKENBY, *The canonical decomposition of once-punctured torus bundles*, Comment. Math. Helv., 78:2 (2003), pp. 363–384.

[20] R. MANDELBAUM, *Branched structures on Riemann surfaces*, Trans. Amer. Math. Soc., 163 (1972), pp. 261–275.

[21] J. MARTINET, *Formes de contact sur les variétés de dimension 3*, Lecture Notes in Math., 209 (1971), pp. 142–163.

[22] W. D. NEUMANN AND D. ZAGIER, *Volumes of hyperbolic three-manifolds*, Topology, 24:3 (1985), pp. 307–332.

[23] J.-P. OTAL, *Le théorème d'hyperbolisation pour les variétés fibrées de dimension 3*, Astérisque, 1:235 (1996), x+159.

[24] R. E. SCHWARTZ, *Real hyperbolic on the outside, complex hyperbolic on the inside*, Invent. Math., 151:2 (2003), pp. 221–295.

[25] R. E. SCHWARTZ, *Spherical CR geometry and Dehn surgery*, volume 165 of *Annals of Mathematics Studies*. Princeton University Press, Princeton, NJ, 2007.

[26] H. SEGERMAN AND S. TILLMANN, *Pseudo-developing maps for ideal triangulations I: essential edges and generalised hyperbolic gluing equations*, in "Topology and geometry in dimension three", volume 560 of Contemp. Math., pp. 85–102. Amer. Math. Soc., Providence, RI, 2011.

[27] W. P. THURSTON, *The geometry and topology of 3–manifolds*. Lecture Notes. 1979.

[28] W. P. THURSTON, *Three-dimensional geometry and topology. Vol. 1*, volume 35 of "Princeton Mathematical Series". Princeton University Press, Princeton, NJ, 1997. Edited by Silvio

Levy.

[29] P. WILL, *Groupes libres, groupes triangulaires et tore épointé dans PU(2,1)*. Theses, Université Pierre et Marie Curie - Paris VI, November 2006.

[30] T. YOSHIDA, *On ideal points of deformation curves of hyperbolic 3-manifolds with one cusp*, Topology, 30:2 (1991), pp. 155–170.